RESEARCH ARTICLE

The nuclear pore Y-complex functions as a platform for transcriptional regulation of *FLOWERING LOCUS C* in Arabidopsis

Penghui Huang[1,2†], Xiaomei Zhang[2†], Zhiyuan Cheng[3†], Xu Wang[4], Yuchen Miao[5], Guowen Huang[6], Yong-Fu Fu[2*] and Xianzhong Feng[1,3*]

[1] Research Institute of Intelligent Computing, Zhejiang Lab, Hangzhou 310012, China
[2] MARA Key Laboratory of Soybean Biology (Beijing), State Key Laboratory of Crop Gene Resources and Breeding, Institute of Crop Sciences, Chinese Academy of Agricultural Sciences, Beijing 100081, China
[3] CAS Key Laboratory of Soybean Molecular Design Breeding, Northeast Institute of Geography and Agroecology, Chinese Academy of Sciences, Changchun 130102, China
[4] Peking University Institute of Advanced Agricultural Sciences, Shandong Laboratory of Advanced Agricultural Sciences at Weifang, Weifang, Shandong 261325, China
[5] State Key Laboratory of Crop Stress Adaptation and Improvement, School of Life Sciences, Henan University, Kaifeng 475004, China
[6] Department of Biological Sciences and Chemical Engineering, Hunan University of Science and Engineering, Yongzhou 425100, Hunan, China

[†] These authors contributed equally to this work.
* Corresponding author: Y.-F.F., fuyongfu@caas.cn; fengxianzhong@iga.ac.cn

Running title: Nuclear Y-complex and *FLC* locus positioning

The author responsible for distribution of materials integral to the findings presented in this article in accordance with the policy described in the Instructions for Authors (https://academic.oup.com/plcell/) is: Yong-Fu Fu (fuyongfu@caas.cn).

Abstract

The nuclear pore complex (NPC) has multiple functions beyond the nucleo-cytoplasmic transport of large molecules. Sub-nuclear compartmentalization of chromatin is critical for gene expression in animals and yeast. However, the mechanism by which the NPC regulates gene expression is poorly understood in plants. Here we report that the Y-complex (Nup107–160 complex, a subcomplex of the NPC) self-maintains its nucleoporin homeostasis and modulates *FLOWERING LOCUS C* (*FLC*) transcription via changing histone modifications at this locus. We show that Y-complex nucleoporins are intimately associated with *FLC* chromatin through their interactions with histone H2A at the nuclear membrane. Fluorescence in situ hybridization assays revealed that Nup96, a Y-complex nucleoporin, enhances *FLC* positioning at the nuclear periphery. Nup96 interacted with HISTONE DEACETYLASE 6 (HDA6), a key repressor of *FLC* expression via histone modification, at the nuclear membrane to attenuate HDA6-catalyzed deposition at the *FLC* locus and change histone modifications. Moreover, we demonstrate that Y-complex nucleoporins interact with RNA polymerase II to increase its occupancy at the *FLC* locus, facilitating transcription. Collectively, our findings identify an attractive mechanism for the Y-complex in regulating *FLC* expression via tethering the locus at the nuclear periphery and altering its histone modification.

IN A NUTSHELL

Background: The nuclear pore complex (NPC) has key functions in transport between the nucleus and the cytoplasm; the NPC is also involved in other nuclear functions, including organization of the nucleus/chromatin, gene expression, and DNA repair in animals and yeast. However, the mechanism by which the NPC functions in regulating gene expression is poorly understood in plants.

Question: How does the NPC regulate expression of the key regulator gene *FLOWERING LOCUS C* (*FLC*) and thus flowering, in Arabidopsis?

Findings: We discovered that the Y-complex self-maintained its nucleoporin homeostasis, allowing *FLC* transcription via changing histone modification patterns at this locus. We found that Y-complex nucleoporins were intimately associated with *FLC* chromatin through their interactions with histone-modifying enzymes at the nuclear membrane. Fluorescence in situ hybridization experiments showed that one of the Y-complex nucleoporins enhanced *FLC* chromatin positioning at the nuclear periphery. Moreover, Y-complex nucleoporins interacted with RNA polymerase II to increase the occupancy of RNA polymerase II at the *FLC* locus, facilitating gene transcription. Collectively, our findings identified an attractive mechanism by which the Y-complex regulates *FLC* gene expression via tethering the locus at the nuclear periphery and altering its histone modification patterns.

Next steps: Our previous findings showed that a nucleoporin from the Y complex participates in photoperiod regulation of flowering through controlling CONSTANS protein stability, therefore it will be interesting to uncover the mechanism by which the Y-complex participates in integrating different flowering pathways. It will also be interesting to elucidate the functions of other NPC sub-complexes in flowering regulation.

Introduction

Beyond nucleo-cytoplasmic transport, the nuclear pore complex (NPC) has been implicated in other nuclear functions, including nuclear organization, gene expression, and DNA repair in animal, yeast (*Saccharomyces cerevisiae*) and plant cells (Gao et al., 2011; Geli and Lisby, 2015; Ibarra and Hetzer, 2015; Ptak and Wozniak, 2016; Gu, 2018; Li and Gu, 2020; Tamura, 2020). Several studies have indicated that histone modifications are associated with the nuclear membrane in animals. For example, the expression of *Paired box 7* (*Pax7*), a fate regulator of myogenic progenitors in mice (*Mus musculus*), is activated in the nucleoplasm but is repressed at the nuclear lamina in a Histone deacetylase 3 (HDAC3)-dependent manner (Demmerle et al., 2013). The nuclear lamina is a meshwork structure beneath the inner nuclear membrane that plays an important role in the regulation of

chromatin organization and gene positioning in eukaryotic organisms (Dechat et al., 2008; Wong et al., 2022), However, there is no evidence for the association of histone modification with the NPC in plants.

The NPC has a highly conserved structure, comprising about 30 different nucleoporins (Nups) that assemble into several sub-complexes (Allen and Douglas, 1989; Goldberg and Allen, 1996; Fiserova et al., 2009; Tamura et al., 2010; Lin and Hoelz, 2019). The Y-complex, also referred to as the Nup107–160 sub-complex, consists of Nup43, Nup85, Nup96, Nup107, Nup133, Nup160, SECRETORY 13 (Sec 13), and SEC13 HOMOLOG 1 (Seh1) in plants (Tamura et al., 2010; Meier et al., 2017). HIGH EXPRESSION OF OSMOTICALLY RESPONSIVE GENES1 (HOS1), a key modulator playing wide functions including in the photoperiodic, circadian clock, and flowering pathways, is also grouped into the classical Y-complex model (Tamura et al., 2010). A HOS1-GFP fusion localizes in both the cytoplasm and the nucleus depending on ambient temperature (Lee et al., 2001; Lee et al., 2012). However, HOS1 interacts with both RNA EXPORT FACTOR 1 (RAE1) and Nup43 and localizes to the nuclear envelope (Reviewed in MacGregor and Penfield, 2015). It was recently shown that HOS1 interacts with Nup96 and Nup160 (Cheng et al., 2020; Li et al., 2020). Therefore, HOS1 functions are closely associated with the NPC. Different Nups of the same sub-complex may function independently or in concert in various aspects of growth and development. Mutation of these *Nup* genes leads to early flowering (Zhang and Li, 2005; Parry et al., 2006; Jacob et al., 2007; Xu et al., 2007; Tamura et al., 2010; Parry, 2014; Xiao et al., 2016; Cheng et al., 2020), at least partially through the photoperiodic flowering pathway (Cheng et al., 2020).

To date, at least four known flowering pathways have been elucidated, and several key integrators of flowering have been identified. *FLOWERING LOCUS C* (*FLC*) is one of these integrators; the autonomous pathway inhibits

FLC expression to accelerate flowering (Koornneef et al., 1991; Koornneef et al., 1998; Simpson, 2004; Hepworth and Dean, 2015; Wu et al., 2020). Therefore, many *flc* mutant alleles, such as the *flc-3* allele generated by fast-neutron mutagenesis, display early flowering (Michaels and Amasino, 1999). Many factors have been shown to regulate *FLC* expression via different mechanisms (Bastow et al., 2004; He et al., 2004; Zhao et al., 2005; Deal et al., 2007; Liu et al., 2007; Cao et al., 2008; Yu and Michaels, 2010; Yu et al., 2011). For example, co-transcriptional coupling between *COOLAIR* (a long antisense RNA expressed from the *FLC* locus) and the state of *FLC* chromatin is critical for the functioning of the autonomous pathway (Berry and Dean, 2015; Whittaker and Dean, 2017). Low *FLC* expression is associated with specific chromatin modifications: low histone acetylation, trimethylation of lysine 4 on histone H3 (H3K4me3) or lysine 36 (H3K36me3), and ubiquitination of histone H2B (H2Bub1), but high H3K27me3 (He et al., 2003; Yang et al., 2014). HISTONE DEACETYLASE 6 (HDA6), a histone deacetylase, and FVE, which is related to Retinoblastoma (Rb), form a complex to mediate histone deacetylation at the *FLC* locus (Ausin et al., 2004; Gu et al., 2011b), while HDA6 directly binds to the *FLC* promoter and represses *FLC* expression (Wu et al., 2008; Yu et al., 2011). HOS1 interacts with FVE and HDA6 to interfere with the FVE–HDA6 association at the *FLC* locus (Jeon and Kim, 2011; Jung et al., 2013). Therefore, HDA6, FVE, and HOS1 form a larger complex on the *FLC* promoter to control gene expression.

Histone H2A has at least 13 variants in Arabidopsis (*Arabidopsis thaliana*), which can be grouped into four clades; accumulating evidence indicates that H2A plays critical roles in gene expression, genome stability, cell cycle progression, DNA repair, recombination, meiosis, and responses to biotic and abiotic stresses (Deal et al., 2007; Talbert and Henikoff, 2010; Lei and Berger, 2020). For example, H2A.Z deposition over genes such as *FLC* is associated with higher transcription (Zilberman et al., 2008; Sura et al., 2017).

In the current study, we show that the Y-complex interacts with histone H2A and participates in histone modification at the *FLC* locus to regulate flowering. Components of Y-complex interact with the histone modifier HDA6 at the nuclear membrane, and mutation of these nucleoporins enhances the association of HDA6 at *FLC* chromatin. In addition, Nup96 tethers the *FLC* locus to the nuclear periphery, and mutation of *Nup96* results in the diminished positioning of the *FLC* locus at the nuclear periphery, leading to repression of *FLC* expression, suggesting that nuclear pore compartmentalization may be key to histone modification at the *FLC* locus to regulate flowering.

Results

Nuclear pore complex homeostasis is self-maintained

Nucleoporin homeostasis is maintained by the relative levels of different nucleoporins typical to the specific cell type and growth conditions (Chow et al., 2014; Parry, 2014; Rajoo et al., 2018; Agote-Aran et al., 2020). We wondered whether the loss of one nucleoporin would influence the stability of other nucleoporins in Arabidopsis. We targeted the Y-complex, consisting of Nup43, Nup85, Nup96, Nup107, Nup133, Nup160, Seh1, and Sec13 in plants (Tamura et al., 2010; Meier et al., 2017), plus HOS1 to investigate this question. Indeed, we detected lower protein levels for Nup96 in nucleoporin mutants (*nup107-3*, *nup160-3*, *nup85-1*, and *hos1-3*) compared to that in wild-type plants by immunoblot (Fig. 1A). The extent of decrease in Nup96 protein abundance in the *hos1-3* and *nup160-3* mutants was more pronounced than in *nup107-3* or *nup85-1* mutant (Fig. 1A). In addition, loss of either Nup160 or Nup96 function also led to stronger effects on HOS1 protein abundance than Nup107or Nup85(Fig. 1B). Examinations of plant development revealed that the observed changes in Nup96 protein abundance are associated with the flowering times of the mutants (Figs. S1A and S1B). Specifically, the loss of

HOS1 or Nup96 resulted in earlier flowering, whereas loss of Nup107 or Nup85 had a weaker effect. Additionally, we generated a transgenic line overexpressing *Nup107-MYC* in wild-type plants and then introduced the *35S:Nup107-MYC* transgene into the *hos1-3*, *nup96-1*, and *nup160-3* mutants by crossing to evaluate the effect of overexpressing a nucleoporin gene on the homeostasis of its encoded protein. We determined that overexpression of *Nup107-MYC* does not lead to the overaccumulation of its encoded protein in *hos1-3*, *nup96-1*, or *nup160-3* (Fig. 1C). Similarly, HOS1-MYC failed to accumulate when overexpressing *HOS1-MYC* in the *nup107-3* mutant, although we did detect high levels of the protein when overexpressed in the wild-type background (Fig. 1D). Therefore, we speculated that nucleoporins are tightly controlled at the protein level. These results are reminiscent of a stoichiometric mechanism for maintaining the structures and functions of the NPC (Wu et al., 2001; Salas-Pino et al., 2017; Rajoo et al., 2018) and suggest that loss of one nucleoporin may initiate a drop in the abundance of other nucleoporin proteins. We further checked the effect of Nup98, a nucleoporin that does not belong to the Y-complex but binds to Nup96 (Griffis et al., 2003; Morchoisne-Bolhy et al., 2015), on the protein stability of Y-complex components with the *nup98a-1 nup98b-1* and *nup98a-2 nup98b-1* double mutants (Jiang et al., 2019; Xiao et al., 2020). Surprisingly, we observed no clear difference for either Nup96 or HOS1 protein abundance between the double mutants and wild-type plants (Fig. 1E), suggesting that different sub-complexes of the NPC have their own independent mechanisms for maintaining homeostasis and potential functional compartmentalization of the NPC.

To understand the mechanism behind protein homeostasis noted above, we tested whether the levels of *Nup* transcripts changed in different mutants: however, we detected no difference in *Nup96* expression among these lines (Fig. 1F), while *HOS1* expression was slightly but significantly higher in

mutants relative to wild-type seedlings (Fig. 1G). Overexpression of *Nup107* in *nup96-1*, *nup160-3*, or *hos1-3* mutants led to lower *Nup107* transcript levels compared to wild type (Fig. 1H), indicating that *Nup107* expression depends on Y-complex components, unlike *Nup96* expression (Fig. 1F). Although *Nup107* transcript levels were lower in Y-complex mutants harboring the *35S:Nup107-MYC* transgene than wild type (Fig. 1H), this difference was much less dramatic than that seen for Nup107 protein abundance (Fig. 1C). *HOS1-MYC* expression was about 50% higher in the *nup107-3* mutant compared to that in the wild-type background (Fig. 1I). A transcriptome deep sequencing (RNA-seq) analysis of different nucleoporin mutants and their wild type (Supplemental Data Set S1) revealed no significant changes in the expression (using a cutoff of |Log2[fold-change]| >1 as being significant) of nucleoporin genes except for *Nup98b* and *RAE1*, which are not members of the Y-complex. Taken together, our data suggest that lower levels of Nup96, HOS1, and Nup107 proteins in these mutants may not result from changes in their transcript levels, but more likely in their protein abundance.

We then asked whether nucleoporins are degraded via the 26S proteasome pathway by treating seedlings with MG132, a specific inhibitor of the 26S proteasome (Huang et al., 2018). Immunoblotting of plant total proteins revealed that MG132 treatment does not increase the abundance of either Nup96 (Fig. S2A) or Nup107 in the wild-type background (Fig. S2B), while MG132 treatment did enhance HOS1 protein accumulation (Fig. S2C). Furthermore, the accumulation of these three proteins in Y-complex mutants did not increase upon MG132 treatment (Fig. S2). Taken together, the protein homeostasis of Nup96 and Nup107 nucleoporins may be independent of the 26S proteasome pathway, while HOS1 protein stability in wild-type plants is related to the 26S proteasome.

In agreement with previous reports of an association between nuclear

structure and nucleoporin levels (Tamura and Hara-Nishimura, 2011), we discovered that mutations in nucleoporin genes alter nuclear morphology from the spindle shape typical of wild-type nuclei to a spherical shape in the *nup96-1*, *hos1-3*, *nup160-3*, *nup85-1*, and *nup107-3* mutants (Fig. 1J). The length of the major axis of nuclei in all these mutants was shorter than that in wild-type plants (Fig. 1K), while the circularity indexes of nuclei in mutant cells were higher than that in wild-type cells (Fig. 1L).

Together, our observations indicate that the change of either the abundance of nucleoporin proteins or nucleus shapes (Figs. 1A, 1B, and 1J-1L) may be associated with flowering time (Fig. S1). To test this hypothesis, we examined the nuclear morphology of multiple flowering time mutants, but we observed no clear changes in their nuclear morphology compared to that of the wild type (Fig. S3), suggesting that flowering time is not generally associated with nuclear morphology. Thus, the protein abundance of nucleoporins may be key to flowering regulation: the lower the protein abundance, the earlier the flowering; alternatively, the building blocks of the Y-complex may be repressors of flowering control.

The Y-complex enhances *FLC* expression through changing histone epigenetic marks at the *FLC* locus

We and other groups have shown that loss of function of nucleoporins leads to clear alterations in plant development, including flowering time (Fig. S1, Zhang and Li, 2005; Parry et al., 2006; Jacob et al., 2007; Xu et al., 2007; Tamura et al., 2010; Parry, 2014; Xiao et al., 2016; Cheng et al., 2020). In the Y-complex, Nup85, Nup96, Nup107, Nup160, and HOS1 are associated with flowering control, and their mutants all flowered earlier than wild type (Figs. S1A and S1B). Indeed, the *nup96-1*, *hos1-3,* and *nup160-3* mutants had similar flowering times in long-day conditions and flowered earlier than the *nup107-3* and *nup85-1* mutants. In addition, the transgenic lines *35S:HOS1-*

279 *GFP*, *35S:Nup96-GFP*, *35S:Nup107-GFP*, and *35S:Nup160-GFP* showed
280 high fluorescent signals of nucleoporin-GFP fusion proteins at the nuclear
281 envelope (Fig. S1C).
282 To analyze the relationship between these nucleoporins and flowering
283 regulation, we carried out an RNA-seq analysis of these gene mutants
284 (Supplemental Data Set S1). As with flowering time (Figs. S1A and S1B),
285 *nup96-1*, *hos1-3,* and *nup160-3* clustered together based on their
286 transcriptomes, while *nup107-3* and *nup85-1* formed a distinct group (Fig.
287 2A). Notably, all mutants shared a highly similar expression patterns with 219
288 genes commonly differentially expressed relative to wild type (100
289 upregulated genes and 119 downregulated genes) (Figs. 2B and S4A). Gene
290 Ontology (GO) term enrichment analysis according to biological process and
291 molecular function revealed that the upregulated DEGs in Y-complex mutants
292 are highly enriched in gene expression processes, including 'DNA binding',
293 'transcription regulator activity', and 'RNA biosynthetic process' (Fig. S4, B
294 and C). Among the common genes, the expression of key flowering activator
295 genes was higher in the mutants, whereas flowering inhibitor genes were
296 repressed compared to the wild type (Fig. 2C). We confirmed these changes
297 in expression for main flowering genes by RT-qPCR analysis: the expression
298 of flowering activators (*FLOWERING LOCUS T* [*FT*] and *SUPPRESSOR OF*
299 *OVEREXPRESSION OF CONSTANS 1* [*SOC1*]) was higher while that of
300 flowering repressors (*FLC*) was lower (Figs. 2D and S5), even across diurnal
301 and developmental patterns (Figs. S6 and S7). Additionally, the expression of
302 *SOC1*, *FT*, and *FLC* returned to wild-type levels in *nup96-1 Nup96pro:Nup96-*
303 *GFP* plants, indicating that the Nup96-GFP fusion is functional and that the
304 changes in gene expression observed above are due to loss of Nup96
305 function (Fig. S8).
306 Because we previously reported that the Nup96–HOS1 module regulates
307 flowering partially through the CO–FT module (Cheng et al., 2020), we
308 investigated another mechanism of the Y-complex flowering pathway in this

study, focusing on the critical flowering repressor *FLC*. To test the genetic relationship between *Nup*s and *FLC*, we generated *nup96-1 flc-3*, *hos1-3 flc-3,* and *nup107-3 flc-3* double mutants by genetically crossing *nup* mutants to *flc-3* (Michaels and Amasino, 1999): all double mutants displayed similar flowering times as their respective *nup* single mutants, which flower earlier than the *flc-3* mutant (Figs. 2E, 2F, and S9). Next, we investigated *FLC* expression and compared it to that of *Nup96*, a nucleoporin gene with a stronger effect on flowering regulation than most other Y-complex members (Figs. S1A and S1B). We determined that the diurnal pattern of expression for *FLC* in the *nup96-1* mutant is significantly lower than in wild type (Fig. 2G). Additionally, *FLC* and *Nup96* shared a common expression trend across early seedling development (Fig. 2H). The results indicate that Nup96 and other Nup107–160 sub-complex components are likely associated with the *FLC* flowering pathway. Since *FLC* belongs to the MADS-box family, we examined the expression of other members in the same clade (*FLOWERING LOCUS M* [*FLM*], *MADS AFFECTING FLOWERING 2* [*MAF2*], *MADS AFFECTING FLOWERING 3* [*MAF3*], *MADS AFFECTING FLOWERING 4* [*MAF4*], and *MADS AFFECTING FLOWERING 5* [*MAF5*]). We established that the expression of these genes except for *MAF4* is lower in the *nup96-1* mutant than in wild type (Fig. S10), suggesting that these genes are also involved in Nup96-mediated regulation of flowering.

FLC functions in the vernalization and autonomous pathways (Simpson, 2004; Hepworth and Dean, 2015; Wu et al., 2020). The Arabidopsis accession used in this study, Columbia (Col-0) flowers normally without the requirement of exposure to low temperature (vernalization). Therefore, we examined the expression levels of the main genes in the autonomous pathway, *FLOWERING CONTROL LOCUS A* (*FCA*), *FPA*, *FLOWERING LOCUS KH DOMAIN* (*FLK*), *FY*, *FLOWERING LOCUS D* (*FLD*), *LUMINIDEPENDENS* (*LD*), and *FVE*, but observed no significant changes in the *nup96-1* mutant

compared to wild type (Fig. S11). SHORT VEGETATIVE PHASE (SVP) is another important flowering suppressor and regulated by signals from the thermosensory, autonomous, and gibberellic acid (GA) pathways (Lee et al., 2007; Li et al., 2008), but *SVP* expression also did not exhibit clear expression changes in the *nup96-1* mutant compared to wild type (Fig. S12A). Additionally, we did not observe significant effects on flowering time when *SVP* was mutated (Fig. S12B) or overexpressed (Fig. S12C) in the *nup96-1* mutant background. Thus, the Y-complex likely participates in flowering regulation in an *FLC*-dependent manner.

Histone epigenetic modification is one of the most important regulatory means of flowering gene expression (He et al., 2003; Yang et al., 2014). Acetylation of histone H3 (H3Ac) and trimethylation (H3K4me3) at *FLC* chromatin enhance *FLC* expression, while H3K27me3 modification represses gene expression (He et al., 2003; Yang et al., 2014). We carried out chromatin immunoprecipitation assays followed by quantitative PCR (ChIP-qPCR) with specific antibodies against H3Ac, H3K4Me3, and H3K27Me3 to detect histone modification states at different sites along the *FLC* locus (Fig. 2I) in wild type and different mutants (*nup96-1*, *hos1-3*, *nup107-3*, *nup160-3*, and *nup85-1*). We determined that activating modifications (H3Ac and H3K4Me3) are present at lower levels (Fig. 2, J and K) while the level of the repressing modification (H3K27Me3) was higher (Fig. 2L) in these mutants compared to wild type. Different mutants displayed alteration of histone modifications at *FLC* chromatin to different degrees, consistent with their flowering times. Generally, H3Ac preferred the P1, P2, P3, and P5 sites (Fig. 2J), while H3K4me tended to prefer the P1, P2, P4, and P5 sites (Fig. 2K). However, H3K27me3 was present at all sites detected (Fig. 2L). The *Nup96pro:Nup96-GFP* transgene complemented the H3Ac epigenetic modification pattern of the *nup96-1* mutant (Fig. S8F). Notably, the change of repressing modifications was stronger than that of activating modifications. Thus, the Y-

complex likely integrates these epigenetic modifications to dictate *FLC* expression.

Y-complex nucleoporins interact with HOS1 to modulate histone modifications at *FLC* chromatin

We previously showed that Nup96 and HOS1 interact and mutually stabilize each other (Cheng et al., 2020). We wondered whether other components of the Y-complex might similarly interact with HOS1. Yeast two-hybrid (Y2H) assays revealed that HOS1 interacts with Nup96, Nup107, and Nup160, but not Nup85 (Fig. 3A). These interaction patterns are consistent with previous reports (Zhu et al., 2017; Cheng et al., 2020; Li et al., 2020). Furthermore, co-immunoprecipitation (Co-IP) assays confirmed the interaction of HOS1 with Nup96, Nup107, and Nup160 in different transgenic Arabidopsis seedlings (Fig. 3B–D). To examine if HOS1 and Nup107 had overlapping distributions in plant cells, we generated *gHOS1-mCherry* (consisting of a genomic fragment encompassing the *HOS1* promoter and coding region) and *35S:Nup107-GFP* transgenic lines. We obtained dual expression lines by crossing *gHOS1-mCherry* to *35S:Nup107-GFP* plants. We detected both Nup107 and HOS1 at the nuclear rim and the two proteins co-localized (Fig. 3E) as HOS1 and Nup96 proteins do (Cheng et al., 2020). We then performed an in vivo bimolecular fluorescence complementation (BiFC) assay by first generating two transgenic lines carrying the transgene *35S:HOS1-YFPc* or *35S:Nup107-YFPn*, before crossing them to obtain transgenic plants harboring both transgenes. In this dual expression line, we observed reconstitution of YFP fluorescence at the nuclear envelope (Fig. 3F), suggesting that Nup107 and HOS1 interact at the nuclear envelope.

HOS1 protein abundance was lower in Y-complex mutants compared to that in wild-type plants (Fig. 1B), even though *HOS1* gene expression was slightly upregulated in *nup96-1*, *nup107-3*, and *nup160-3* mutants (Figs. 1F and S13).

Additionally, consistent with the flowering phenotypes (Fig. 3, G and H), the levels of *FLC*, *SOC1*, and *FT* transcripts in the *nup96-1 hos1-3* double mutant were similar to those in the *hos1-3* and *nup96-1* single mutants (Figs. 3I and S7), and the histone modifications at *FLC* chromatin in the single and double mutants were quite similar (Fig. 3J–L). The results suggest that the Y-complex interacts with HOS1 and is associated with changes in histone modifications at *FLC* chromatin.

The Y-complex attenuates HDA6 binding to *FLC* chromatin

HDA6 is an epigenetic integrator that catalyzes histone deacetylation and methylation (Kim et al., 2012; Liu et al., 2012a). We investigated the relationship between Nup96 and HDA6 by generating two transgenic lines expressing *Nup96-YFPn* or *HDA6-YFPc* and crossed them to obtain transgenic plants expressing both *Nup96-YFPn* and *HDA6-YFPc*. In these lines, we observed reconstitution of YFP fluorescence signal via BiFC exclusively at the nuclear membrane (Fig. 4A), indicating that Nup96 interacts with HDA6 at the nuclear membrane. We also detected the individual proteins, Nup96-GFP (Fig. S1C) and HDA6-GFP (Fig. 4B), at the nuclear rim in their respective transgenic lines. To confirm the above observation, we purified the nuclear membrane fraction from *HDA6pro:HDA6-GFP* seedlings and established that HDA6 co-purifies with Nup96 (Fig. 4C). We also detected an interaction between Nup96 and HDA6 in Arabidopsis plants overexpressing *HDA6* by Co-IP assays (Fig. 4D). In addition, both Nup107 and Nup160 also interacted with HDA6 (Figs. 4E and 4F) in *N. benthamiana* leaves. HOS1 was previously reported to interact with HDA6, acting as an antagonist of the association of the HDA6–FVE co-repressor complex to the *FLC* locus (Jung et al., 2013; Hepworth and Dean, 2015). To test whether Nup96, HOS1, and HDA6 might form a complex in vivo, we carried out a Co-IP assay with a *35S:HDA6-MYC* transgenic line and an anti-MYC antibody, we observed that HDA6 can immunoprecipitate Nup96 and HOS1 (Fig. 4G),

indicating that Nup96, HOS1, and HDA6 all interact with one another in planta. A similar result was observed in a recent study (Niu et al., 2022), showing that several nucleoporins specifically co-precipitated with HDA9 from plant protein extracts. In addition, HDA9 and HOS1 co-exist at the nuclear envelope. Therefore, histone deacetylases such as HDA6 and HDA9 interact preferentially with components of the Y-complex at the NPC.

HDA6 exhibited a similar mRNA abundance in different mutants of the Y-complex (Fig. S14A). We also did not detect differences in HDA6-GFP protein abundance among different backgrounds including wild-type plants and *hos1-3, nup96-1* and *nup160-3* mutants (Fig. 4H), indicating that the Y-complex does not regulate *HDA6* expression or HDA6 protein stability. Therefore, we asked if the Y-complex influences HDA6 occupancy at *FLC* chromatin. Using the *HDA6pro:HDA6-GFP* transgenic lines and an anti-GFP antibody, we determined that the abundance of HDA6-GFP is higher at the P1 and P2 regions of *FLC* chromatin in the *hos1-3*, *nup96-1*, and *nup160-3* mutants compared to in wild type (Fig. 4I). In summary, these results suggest that the Y-complex interacts with HDA6 to attenuate its binding to *FLC* chromatin, which in turn enhances *FLC* expression.

Nup96 functions in FVE-mediated histone modification of *FLC* chromatin

To test whether the Nup96 regulation of *FLC* chromatin modifications was influenced by FVE, we examined the effect of mutations in the Y-complex on *FVE* expression. We detected no significant changes for *FVE* expression in different mutants of the Y-complex compared to wild type (Fig. S14B). The *fve-3 nup96-1* double mutant flowered later than the *nup96-1* mutant but earlier than the *fve-3* mutant (Fig. 5, A and B), and *FLC* expression levels in these mutants coincided with their flowering phenotypes (Fig. 5C). We also examined histone modification at the *FLC* locus in these genotypes. The changes in histone modifications (H3Ac, H3K3me3, and H3K27me3) at the

FLC locus were similar in the double mutant and *fve-3* (Fig. 5D–F). Thus, Nup96 regulates the modification of *FLC* chromatin at least partially through FVE, as does HOS1 (Jung et al., 2013; Hepworth and Dean, 2015).

The Y-complex is intimately associated with *FLC* chromatin

The results above clearly showed that the Y-complex regulates *FLC* expression by changing chromatin status. Thus, we were interested in checking if the Y-complex might interact directly with chromatin. We therefore carried out a Co-IP assay with and anti-histone H2A antibody using wild-type seedlings, which revealed that HOS1 co-immunoprecipitates with histone H2A (Fig. S15A). We also determined that HOS1, Nup96, and Nup107 interact with histone H2A variants (HTA6, HTA9, and HTA13, belonging to different phylogenetic classes (Lei and Berger, 2020)) via BiFC assays throughout the entire nuclei of *N. benthamiana* leaves (Figs. 6A–C and S16–18). Considering that Y-complex components may not be located correctly at the nuclear membrane in the transient expression system of *N. benthamiana* leaves (Fig. S19A), the position of the interaction with these interacting proteins might be changed. To resolve this issue, we added a transmembrane domain (TMD) from the Arabidopsis KASH protein WPP DOMAIN INTERACTING PROTEIN 1 (WIP1) (Zhou et al., 2012; Groves et al., 2019) to the C terminus of Nup96. Importantly, the resulting chimeric protein GFP-Nup96-TMD localized to the nuclear membrane (Fig. S19B). Using this fusion protein (Nup96-TMD), we observed that Nup96 interacts with HTA6, HTA9, and HT13 at the nuclear membrane by BiFC assays (Fig. 6D), indicating that Nup96-interacting proteins re-position themselves at the nuclear membrane when Nup96 localized to this nuclear sub-section. In addition, HTA9 co-precipitated HOS1 (Fig. 6E), Nup96 (Fig. 6F), and Nup107 (Fig. 6G) from Arabidopsis total protein extracts, using an antibody against HTA9. These results indicate that the Y-complex is intimately associated with chromatin. However, the Y-complex did not affect the stability of either histone H2A or HTA9 (Figs. 6H, 6I

and S15C). In addition, we did not detect a physical interaction between histone H2A and Y-complex components in Y2H assays (Fig. S15B), suggesting that some specific intermediate factors from Arabidopsis cells may be required for such an association, or that Y-complex components may interact with histone H2A in specific contexts of epigenetic modifications.

FLC locus positioning is regulated by the Y-complex in the nucleus

We speculated that the Y-complex may tether *FLC* chromatin to the NPC and affect it transcriptional activity. To test this hypothesis, we used ChIP-qPCR to investigate the interaction between Nups and the *FLC* locus. We determined that Nup96, Nup107, and HOS1 can bind to *FLC* chromatin at the P1 and P2 regions of the *FLC* locus in different transgenic plants (Fig. 7, A and B).

Binding of RNA polymerase II (RPB) to chromatin is a requisite for transcription. Thus, we analyzed the relationship between the Y-complex and RPB. We detected a strong interaction of RPB2 (RNA polymerase II subunit 2) with HOS1 and a weak interaction with Nup107 in Co-IP experiments using an anti-RPB2 antibody (Fig. 7, C and D). Surprisingly, the band of HOS1 that was co-precipitated by RPB2 corresponded to ubiquitin-modified HOS1 (Fig. 7C, lowest row). However, the Y-complex did not have any effects on the stability of RPB2 (Fig. 7E). To confirm the repressed state of *FLC* expression in Y-complex mutants (Fig. 2D), we compared RNA polymerase II (RNA Pol II) occupancy at the *FLC* locus among wild-type plants and different *nup* mutants using an antibody against RNA polymerase II subunit RPB1 in a ChIP-qPCR assay. RNA Pol II occupancy at *FLC* was significantly lower in *nup* mutants than in wild type (Fig. 7F), leading to lower *FLC* expression (Fig. 2D), suggesting that the Y-complex regulates *FLC* transcription.

Finally, we asked whether the direct interaction between the Y-complex and the *FLC* gene occurred at the nuclear periphery by fluorescent in situ

hybridization (FISH) analyses (Fig. 7G–I). According to previously described methods (Feng et al., 2014; Sakamoto et al., 2020), we defined the area within 0.2 μm of the nuclear edge as the nuclear periphery. Interestingly, the percentages of nuclei in which the *FLC* locus was at the nuclear periphery was significantly lower in the *nup96-1* mutant (19.9±1%) compared with that in wild type (24±2%) (Fig. 7, H and I). These results suggest that Nup96 mediates the positioning of the *FLC* locus at the nuclear periphery. Collectively, the Y-complex may recruit *FLC* chromatin to the NPC, mediated by chromatin proteins, such as histone H2A and RNA polymerase II, thus contributing to the regulation of gene expression.

Discussion

NPC self-maintains its own stoichiometry

Different Nups maintain NPC stoichiometry or quality control for normal cellular functions (Gall, 1967; DeGrasse et al., 2009; Tamura et al., 2010). Altering Nup abundance leads to abnormal NPCs with pronounced changes in stoichiometry (Rajoo et al., 2018). Our data show that loss of function of an individual Nup in the Y-complex results in a lower abundance of other Nups in the same sub-complex, which cannot be rescued by overexpressing an individual *Nup* gene in other *nup* mutants (Fig. 1). However, RT-qPCR and RNA-seq analyses revealed that no significant changes in their transcript levels in these mutants (Fig. 1 and Supplemental Data Set S1), consistent with studies in animals (Chakraborty et al., 2008). Our results clearly indicate a stoichiometric balance among different Nups of Y-complex that is self-maintained and coordinated at the protein levels rather than at the transcriptional level. The degree of changes in Nup protein abundance is correlated with their inhibitory functions in flowering. For example, the abundance of Nup96 in the *nup160-3* mutant was lower than in the *nup107-3* mutant; moreover, the *nup160-3* mutant flowers earlier than *nup107-3* (Figs. 1 and S1, A and B). Such a stoichiometric change in the Nup107–160 complex

549 also supports the hypothesis of compositional plasticity of NPC architecture,
550 with some components being dispensable for basal growth (Rajoo et al.,
551 2018), since single mutants in the Nup107–160 complex can fulfill their entire
552 life cycle even though some mutants display abnormal phenotypes (Fig. S1A).
553 However, different sub-complexes have their own independent balancing
554 mechanisms, as the loss of Nup98, a non-component in Y-complex, did not
555 affect the abundance of other Y-complex proteins (Fig. 1E), suggesting that
556 functional compartmentalization of the NPC may be important for functions of
557 different NPC sub-complexes. In addition, the degradation of Y-complex
558 proteins was independent of the 26S proteasome pathway, as MG132
559 treatment did not result in the accumulation of Y-complex proteins in the
560 mutants (Fig. S2).
561
562 Nuclei vary in size and shape depending on the tissues and environmental
563 conditions (Chytilova et al., 2000), and changes in the abundance of a single
564 nucleoporin will alter nuclear structure (Wong et al., 2015; Meier et al., 2017;
565 Goto et al., 2021). Mutation of *Nup96*, *Nup160*, *HOS1*, *Nup107*, or *Nup85* all
566 led to a short major axis and more circular nuclei (Fig.1J–L), consistent with
567 previous reports (reviewed in Meier et al., 2017).
568 This result is not surprising, because the conserved Nup107–160 complex
569 plays key roles in NPC assembly through NPC interconnection (Walther et al.,
570 2003) and NPC interconnects with the nuclear lamina, one of the control
571 points for nuclear integrity (Wong et al., 2022). Interestingly, *nup* mutants with
572 early flowering phenotypes have more circular nuclei than wild type plants.
573 However, the nuclear morphology of other flowering time mutants not related
574 to the NPC was similar to that of the wild type. A previous report showed that
575 mutation of the gene *CROWDED NUCLEI* (*CRWN1* or *4*) leads to a strong
576 change in nuclear morphology but has no effect on flowering time (Dittmer et
577 al., 2007). Thus, there may be no direct relationship between nuclear
578 morphology and flowering time.

Nucleoporins in the Y-complex function as one entity, but not equally

The Nup107–160 complex functions as one entity in mitosis (Loiodice et al., 2004). Mutants of components of the Y-complex have similar phenotypes in plants, including early flowering (Fig. S1) (Tamura et al., 2010; Parry, 2014; Cheng et al., 2020). Loss of an individual Nup leads to lower protein abundance for other members in the same sub-complex (Fig. 1) and the histone H2A variants and HDA6 interact with all constituent Nups detected (Figs. 4 and 6), suggesting the importance of maintaining complex integrity and their common function in the regulation of *FLC* expression. In addition, transcriptome analysis of mutants in Y-complex components revealed that all mutants shared high similarity in their differentially regulated genes, with 219 DEGs in common (Fig. 2B).

However, in terms of protein accumulation, nuclear morphology, transcriptome, and flowering time, Nup85 and Nup107 may behave differently from HOS1, Nup96, and Nup160, possibly due to their spatial locations in the Y-complex. In addition, different sub-complexes may have specific functions or mechanisms within the same stages of development, as Nup98 does not affect the abundance of other Y-complex constituent Nups (Fig.1). We also showed that Nup98 regulates flowering independently from CONSTANS (CO) (Jiang et al., 2019), while Nup96 controls CO protein degradation in the photoperiodic flowering pathway (Cheng et al., 2020). Mutation of constituent Nups results in changes in flowering times to different degrees (Fig. S1), suggesting that different constituent Nups may have distinct effects.

The Y-complex is a functional site for *FLC* transcriptional regulation

Mutation of Y-complex does not affect the abundance of RNA pol II (Fig. 7E), but decreases its occupancy at the *FLC* locus (Fig. 7F), suggesting that the Y-complex is associated with *FLC* expression (Fig. 2) at least partially through

controlling how much RNA pol II is retained at *FLC* chromatin. A previous report showed that LacI-YFP (a fusion between the Lac repressor and YFP) activity lead to higher transcription of a luciferase reporter gene with the Lac operator upstream of it when LacI-YFP is fused to Seh1, but decreases when fused to Nup50a (a non-Y-complex component) (Smith et al., 2015). Similar characteristics have previously been reported in animals (Kuhn and Capelson, 2019; Gozalo et al., 2020). Thus, the functions of Y-complex Nups in gene expression are conserved across eukaryotic taxa (D'Angelo, 2018).

During animal cell differentiation, maturation, and tissue development, the positioning of genes is actively regulated and affects their expression levels (Kosak et al., 2002; Ragoczy et al., 2006; Meister et al., 2010). It was reported that light triggers a rapid repositioning of the Arabidopsis *CHLOROPHYLL A/B-BINDING* (*CAB1/2/3*) locus from the nuclear interior to the nuclear periphery during its transcriptional activation (Feng et al., 2014). Another study on the localization of *FLC* copies suggests that gene repositioning is also involved in gene expression in Arabidopsis (Rosa et al., 2013). However, the molecular mechanism by which gene repositioning affects gene expression has not been elucidated.

Emerging evidence has revealed a new mechanism by which nucleoporins directly bind to chromatin to regulate gene expression in different organisms (Vaquerizas et al., 2010; Jacinto et al., 2015; Gao et al., 2021). However, what happens in plants is unclear, although Tang et al (2021) reported that PLANT NUCLEAR ENVELOPE TRANSMEMBRANE 2 (PNET2) (a true inner nuclear membrane protein, not a nucleoporin) is intimately associated with chromatin. A recent elegant study showed that CRWNs, lamina binding proteins located at the inner nuclear membrane (INM), regulate the position of the *COPPER-ASSOCIATED* (*CA*) locus as a function of copper concentration, suggesting that gene repositioning is involved in gene activation in Arabidopsis

(Sakamoto et al., 2020). Our study indicates that Nup96 tethers the *FLC* locus to the nuclear periphery (Fig, 7G–I), and that mutation of *Nup96* results in a decrease of in the positioning of *FLC* at the nuclear periphery and repression of *FLC* expression, indicating that Y-complex-dependent gene positioning is associated with *FLC* gene activity. We determined that the Y-complex can interact with histone H2A variants (Figs. 6 and S15–S18), the histone deacetylase HDA6 (Fig. 4), and RNA pol II (Fig. 7, C and D). In addition, HDA6 and histone H2A interact with Nup96 at the nuclear envelope (Figs. 4A and 6D). Similar results were observed in a recent study, in which several nucleoporins specifically co-precipitated with HDA9 and the HDA9–HOS1 complex existed at the nuclear envelope (Niu et al., 2022). Nup96, Nup107, and HOS1 were enriched at the *FLC* chromatin in ChIP-qPCR assays (Fig. 7, A and B), consistent with a previous report for HOS1 (Jung et al., 2013). Another key histone deacetylase, FLD, forms a complex with FVE and HDA6 to modulate histone epigenetic modifications at the *FLC* locus (Gu et al., 2011a; Yu et al., 2011; Yu et al., 2016). However, HOS1 interacts with both FVE and HDA6 proteins, but not FLD (Jung et al., 2013; Hepworth and Dean, 2015), and we did not detect any change for *FLD* expression in the *nup96* mutant. Thus, whether FLD is involved in the Y-complex functions reported here remains to be uncovered.

Transcriptome analysis of Y-complex mutants revealed that all mutants shared common DEGs, including genes associated with DNA binding, transcription regulator activity, and RNA biosynthesis (Fig. S4), further indicating that the Y-complex plays an important role in regulating gene expression. Therefore, our results provide a new line of evidence that the Y-complex directly binds to *FLC* chromatin to regulate *FLC* transcription.

Collectively, we propose a model for Y-complex-mediated regulation of flowering via modification of the *FLC* locus (Fig. 8). In wild-type plants, an

intact Y-complex recruits *FLC* chromatin to the NPC via interacting with histones, and then attenuates the epigenetic modulator HDA6 to bind to the *FLC* locus to deacetylate local histones, facilitating the enrichment of RNA Pol II to chromatin and resulting in *FLC* transcription. In mutants of the Y-complex, the recruitment of *FLC* chromatin is obstructed, and the histone modification pattern on the chromatin far away from the nuclear envelope changes, leading to inhibition of *FLC* transcription and finally early flowering.

Materials and Methods

Plant Materials and Growth Conditions

Seeds of the T-DNA insertion mutants of *Arabidopsis thaliana hos1-3* (SALK_069312), *nup96-1* (SALK_109959), *nup107-3* (SALK_057072), *nup160-3* (SALK_133728C), and *nup85-1* (SALK_113274) were obtained from the ABRC (Ohio State University). Screening of homozygous mutants was performed according to the protocol provided by Signal SALK (http://signal.salk.edu/). Other mutants were described previously: *fve-3* (Ausin et al., 2004) and *flc-3* (Seo et al., 2009). The double mutants *nup98a-1 nup98b-1* and *nup98a-2 nup98b-1* (Xiao et al., 2020), *hos1-3 nup96-1* (Cheng et al., 2020), *hos1-3 flc-3*, *nup96-1 flc-3*, *nup107-3 flc-3* and *nup96-1 fve-3* (this study) were obtained via genetic crossing. Seeds were surface sterilized (washed in 70% [v/v] ethanol for 6 min, 100% [v/v] ethanol for 1 min) and stratified for 3 days at 4°C on 1/2×Murashige and Skoog (MS) medium solidified with 0.75% (w/v) agar before being transferred to a controlled culture room at 22°C, with a 16-h light/8-h dark photoperiod Green Power LED top lighting (Philips Horticulture LED), with an intensity of 250 $\mu molm^{-2}$ s^{-1} for 10 days before transplanting into soil (PINDSTRUP SPHAGNUM [0-6 mm, Denmark]: vermiculite = 3:1) for further growth. For measuring flowering time, the number of rosette leaves were counted when plants were bolting about 1 cm. At least 18 plants were counted and their data averaged for each

measurement.

Gene Expression Analysis

Total RNA was isolated from 10-day-old seedlings using a Hipure Plant RNA Mini Kit (Magen, R4151-02, China) according to the manufacturer's instructions. RNA preparation, RT-qPCR, and data processing were performed as described previously (Cheng et al., 2020). *TIP41* was used as the internal control for RT-qPCR (Gutierrez et al., 2008). All primer sequences are listed in Supplemental Table S1.

Hoechst Staining

Hoechst staining experiments were performed according to a previously described method (Tamura et al., 2010). The nuclei in rosette leaves from 14-day-old wild-type and mutants seedlings grown at 22°C were stained for 30 min at room temperature with 1 μg/mL Hoechst 33342 solution (3.7% [w/v] paraformaldehyde, 10% [v/v] DMSO, 3% [v/v] Nonidet P-40, 50 mM PIPES-KOH pH 7.0, 1 mM $MgSO_4$, and 5 mM EGTA). The stained nuclei were observed using a confocal laser scanning microscope (LSM 700, Carl Zeiss). At least 30 nuclei were photographed, and the data were analyzed using ImageJ (http://rsbweb.nih.gov/ij/).

RNA-seq and Data Analysis

Three batches of 12-day-old wild-type, *hos1-3*, *nup85-1*, *nup96-1*, *nup107-3*, and *nup160-3* seedlings grown in long-day conditions were harvested at zeitgeber time 15 (ZT15, 1 h before lights-off) and used for total RNA extraction. The quality of RNA samples was analyzed with a Nanodrop 2000 Bioanalyzer (Agilent). Barcoded cDNA libraries were prepared using Illumina Poly-A Purification TruSeq library reagents and protocols. Samples of three biological repeats were sequenced on Illumina HiSeq 2500 V4 (paired-end

125-bp run). The paired-end reads were aligned to the TAIR10 genome using tophat-2.0.11. Relative transcript abundance was normalized and presented as fragments per kilobase of transcript per million mapped reads (FPKM). Differentially expressed genes were identified using DEseq2 with an absolute Log2(FC) > 1 and $p < 0.01$ as criteria. To obtain insight into the flowering time changes seen in mutants, the expression of 21 flowering-related genes acquired from the Flowering Interactive Database (Bouche et al., 2016) was analyzed and heatmap was displayed using the R package pheatmap (v1.0.12) (https://cran.r-project.org/web/packages/pheatmap/index.html). RNA-seq data were submitted to the National Center for Biotechnology Information with Sequence Read Archive (SRA) data accession number PRJNA1027589.

Stable Expression of GFP Fusions in Arabidopsis

To generate the *HDA6pro:HDA6-GFP* construct, a 2.7-kb genomic sequence upstream of the *HDA6* start codon was cloned into the pFu76 vector (Wang et al., 2013) resulting in a *HDA6* promoter entry clone. The entire *HDA6* coding region excluding the translation termination codon was amplified by PCR using first-strand cDNA prepared from Col-0 RNA as the template was cloned into pFu28 (Wang et al., 2013) to produce a *HDA6-GFP* gene entry clone. These two plasmids were integrated into the destination vector pFu39-2 (Wang et al., 2013) to generate a *HDA6pro:HDA6-GFP* binary vector. The constructs *35S:HOS1-GFP*, *35S:Nup96-GFP*, *35S:Nup107-GFP*, and *35S:Nup160-GFP* were transformed into Col-0 plants. These constructs were introduced into Agrobacterium (*Agrobacterium tumefaciens*) strain GV3101 and transformed into Col-0 plants by the floral dip method.

Immunoblot Assays

Seedlings grown under long-day conditions for 10 days were harvested and

ground to a fine powder in liquid nitrogen. Nuclear proteins were extracted as previously described (Hayama et al., 2017; Cheng et al., 2020). In brief, 0.1 g of powder was mixed with 800 μL of nucleoprotein extraction buffer (20 mM Tris-HCl, pH 6.8, 20 mM $MgCl_2$, 5% [w/v] sucrose, 40% [v/v] glycerol, 0.3% [v/v] Triton X-100, 0.08% [v/v] *β*-mercaptoethanol, 1 × protease inhibitor mixture, 1 mM DTT, and 1.3 mM PMSF). After centrifugation at 4500 × *g* for 7 min at 4°C, the supernatant was discarded. The pellet was washed with nucleoprotein extraction buffer four times. Finally, the pellet was heated at 98°C for 10 min in 2 × SDS-PAGE loading buffer and centrifuged at 14,000 × *g* for 10 min at room temperature. The supernatant was used for immunoblotting. Different primary antibodies were used for probing blots. Anti-Nup96 antibody (1:1000), anti-HOS1 antibody (1:1000) (Cheng et al., 2020), anti-RPB2 antibody (1:1000) (PHY2429S, PHYTO AB), anti-H2A antibody (1:2000) (A20315, ABclonal), and anti-HTA9 antibody (1:2000) (A17304, ABclonal) were used. Anti-Nup96 antibody and anti-HOS1 antibody were used as described previously (Cheng et al., 2020). Signals on blots were quantified using ImageJ software.

Protein–Protein Interaction Assays

Bimolecular fluorescence complementation (BiFC) assays were performed as described previously (Cheng et al., 2020). The full-length *HOS1*, *Nup96*, *Nup107*, *Nup160*, *Nup85*, and *HDA6* coding sequences were individually cloned into the pGWC vector (Chen et al., 2006), and the full-length *SUN1*, *HTA6*, *HTA9*, and *HTA13* coding sequences were cloned into the pDONR207 vector. All resulting clones were confirmed by Sanger sequencing, then recombined into the BiFC binary vectors pEarlygate201-YFPn or pEarlygate202-YFPc (Earley et al., 2006) by LR Clonase (Invitrogen™, 11791020). These constructs were introduced into Agrobacterium (*Agrobacterium tumefaciens*) strain GV3101, which was infiltrated into the leaves of 4-week-old *Nicotiana benthamiana* plants. After 40 to 48 h, YFP

fluorescence was visualized under a confocal microscope. To evaluate whether the Nup96–HDA6 interactions occurred in vivo, *35S*:*Nup96-YFPn* and *35S*:*HDA6-YFPc* were separately transformed into Col-0 plants. The two resulting transgenic lines were crossed to generate plants harboring both *35S*:*Nup96-YFPn* and *35S*:*HDA6-YFPc*; these plants were used to detect the signal of reconstituted YFP fluorescence by laser scanning confocal microscopy (LSM 700, Carl Zeiss). Yeast two-hybrid (Y2H) assays were performed following the Matchmaker GAL4 two-hybrid system (Clontech). Y2H Gold yeast strain co-transformed with pGADT7-Nups+pGBKT7, pGADT7+pGBKT7-HOS1, and pGADT7-Nups+pGBKT7-HOS1, with the AD+BD pair used as negative control. Potential interactions were assayed on synthetic defined (SD) medium lacking Leu, Trp, His, and Ade (SD/−4). Co-immunoprecipitation (Co-IP) assays were performed as described previously (Cheng et al., 2020). To evaluate whether the HDA6, Nup96, and HOS1 interactions occur in vivo, *35S:HDA6-MYC* transgenic lines in the Col-0 background were used and were kindly provided by Dr Keqiang Wu (Liu et al., 2012b).

ChIP-qPCR Assay

ChIP experiments were performed as described previously (Saleh et al., 2008). Briefly, 10-day-old seedlings (1 g fresh weight) grown on MS agar plates under long-day conditions were collected for chromatin extraction. Sonicated chromatin was immunoprecipitated with anti-RNA Pol II (RPB1, Agrisera, AS111804), anti-H3Ac (Abcam, ab47915), anti-H3K4Me3 (Abcam, ab1012), anti-H3K27Me3 (Abcam, ab6002), anti-GFP (Abcam, ab290), anti-MYC (Millipore, 06-340) antibodies. The *eIF4A* gene was used for normalizing the quantified DNA fragments (Jung et al., 2013). All primers used in the ChIP-qPCR are listed in Supplemental Table S1.

Protoplast Isolation and Nuclear Envelope Extraction

Protoplasts were isolated from rosette leaves of *HDA6pro:HDA6-GFP* transgenic seedlings grown on MS agar plates for 14 days as described previously (Jung et al., 2015). Nuclear envelope isolation was performed as previously described (Liu et al., 2019) with slight modifications. Briefly, around 10^6–10^7 protoplasts were mixed with 0.5 mL buffer A (Inventbiotech, NE-013) with 1 × protease inhibitor mixture (Roche). After 10 min on ice, the extract was mixed thoroughly. Then, the extract was transferred to the filter cartridge and centrifuged at 14,000 × *g* for 30 s at 4°C. The supernatant was saved as a cytosol. The pellet (nuclei) was washed twice with 1 mL cold phosphate-buffered saline (PBS) with 1 × protease inhibitor mixture (Roche). Next, 0.3 mL of buffer B (Inventbiotech, NE-013) with 1 × protease inhibitor mixture (Roche) was added to the pellet, and then mixed thoroughly. After 5 min on ice, the extract was vigorously vortexed for 10 s and incubated again for 5 min on ice and vigorously vortexed for 10 s. Eighty microliters of the supernatant were saved as the nuclear fraction. After centrifugation at 6000 × *g* for 5 min at 4°C, the supernatant was transferred to a fresh 2.0-mL microcentrifuge tube. Then, 800 μL cold PBS with 1 × protease inhibitor mixture (Roche) was added to the tube, which was inverted 10 times. Centrifugation was then performed at 16,000 × *g* for 15 min at 4°C. Nuclear envelope proteins (NEs) were finally resuspended in 70 μL 2 × SDS loading buffer and boiled at 98°C for 10 min. Nup96 was used as a positive control for the nuclear envelope fraction; Histone H3.1 (Abmart, P30266, China) was used as a positive control for the nuclear fraction, and Actin (Abmart, M20009L, China) was used as a positive control for the cytoplasmic fraction.

Fluorescence in situ hybridization

Tissue fixation and isolation of nuclei were performed based on previous protocols (Feng et al., 2014; Sakamoto et al., 2020) and fluorescence in situ hybridization was conducted based on a previous report (Rosa et al., 2016) with modifications. Approximately 30 10-day-old seedlings were fixed with

cold fixation buffer (4% [w/v] formaldehyde, 10 mM Tris-HCl pH 7.5, 10 mM EDTA, and 100 mM NaCl) for 20 min under a vacuum and then 2 M glycine was added (final concentration, 150 mM). The seedlings were chopped in 50 µL of lysis buffer (15 mM Tris-HCl pH 7.5, 2 mM EDTA, 0.5 mM spermine-4 HCl (Sigma, S2876), 80 mM KCl, 20 mM NaCl, and 0.1% [v/v] Triton X-100) with a razor blade on a glass slide. The chopped sample containing the released nuclei was transferred into 400 µL of nuclei suspension buffer (100 mM Tris-HCl pH 7.5, 50 mM KCl, 2 mM $MgCl_2$, 5% [w/v] sucrose and 0.05% [v/v] Tween-20) and then the solution was filtered through a 40-µm cell strainer. The nuclear suspension was spotted onto a slide and allowed to dry overnight. The cover slides were either used immediately or stored at −20°C. Slides were treated with 100 µg mL^{-1} RNase for 30 min at 37°C and washed twice in 2 × SSC. After washing, the slides were re-fixed with 4% (w/v) formaldehyde freshly made from paraformaldehyde in PBS for 10 min. After washing the slides in ddH_2O for 5 min, nuclei were then transferred to a series of cold ethanol steps increasing to 70%, 90%, and 100% (5 min each, all v/v). The slides were soaked in SF (70% [w/v] formamide in 2 × SSC) for 2 min at 76°C. Subsequently, the slides were incubated in a series of cold ethanol steps increasing to 70%, 90%, and 100% (5 min each, all v/v). Bacterial artificial chromosome clone JAtY71K18 (Rosa et al., 2016) was used as a probe. Probes were labeled with digoxigenin-11-dUTP (#11745816910, Roche) by nick translation. To denature the labeled DNA, the hybridization mixture (20 ng $µL^{-1}$ labeled DNA, 50% [w/v] formamide, 10% [w/v] dextran sulfate, 2 × SSC, 1 mg mL^{-1} salmon sperm) was placed on a heating block for 10 min at 85°C and applied to the slides. Slides covered with the hybridization mixture were hybridized overnight at 37°C. After hybridization, the slides were washed at 42°C once in 2 × SSC, twice in 2 × SSC at room temperature, twice in 4 × SSC plus 0.2% (v/v) Tween-20 at room temperature. The slides were then blocked in TNB (0.1 M Tris-HCl, 0.15 M NaCl, 3% [w/v] BSA) for 30 min at 37°C. Digoxigenin probes were detected with a rhodamine-anti-

digoxigenin (#11207750910, Roche) prepared in TNB buffer (1:100) for 1 h at 37°C. Nuclei were counterstained with 1 μg mL^{-1} DAPI.

Statistical Analyses

At least three biologically independent samples were used in this study. All statistical analyses were performed using the SPSS software package. A two-tailed Student's *t* test (*, $P < 0.05$) was used to determine the statistical significance of differences between two means. One-way analysis of variance (ANOVA) (*, $P < 0.05$) was used to analyze statistical significance for more than two groups of samples. Detailed statistical analysis data are shown in Supplemental Data Set S2.

Accession Numbers

Sequence data from this article can be obtained from in the GenBank/EMBL databases under the following accession numbers: *HOS1* (At2g39810), *Nup96* (At1g80680), *Nup85* (At4g32910), *Nup107* (At3g14120), *Nup160* (At1g33410), *Nup98a* (At1g10390), *Nup98b* (At1g59660), *FLC* (At5g10140), *FLM* (At1g77080), *MAF2* (At1g77080), *MAF3* (At5g65060), *MAF4* (At5g65070), *MAF5* (At5g65080), *FCA* (At4g16280), *FPA* (At2g43410), *FLK* (At3g04610), *FY* (At5g13480), *FLD* (At3g10390), *LD* (At4g02560), *SVP* (At2g22540), *CO* (At2g22540), *FT* (At1g65480), *SOC1* (At2g45660), *HDA6* (At5g63110), *FVE* (At2g19520), *HTA6* (At5g59870), *HTA9* (At1g52740), *HTA13* (At3g20670), *SUN1* (At5g04990), *TIP41* (At4g34270), and *eIF4A* (At3g13920).

Acknowledgments

We thank Dr Jose Miguel Martinez-Zapater (Departamento de Genética Molecular de Plantas, Centro Nacional de Biotecnología, Consejo Superior de Investigaciones Científicas, Campus de la Universidad Autónoma de Madrid) for kindly providing *fve-3* mutant seeds, Dr Peter Huijser (Department of Comparative Development and Genetics, Max Planck Institute for Plant Breeding Research) for kindly providing *svp-41* mutant seeds, and Dr Keqiang Wu (College of Life Science, National Taiwan University) for kindly providing seeds of *35S*:*HDA6-MYC* in Col-0 background. We thank Dr Faqiang Wu for his help in the drawing of the model. This work was supported by the National Natural Science Foundation of China (30670189, 31370324, and 31571411). We thank LetPub (www.letpub.com) for linguistic assistance during the preparation of this manuscript.

Author contributions

Y.-F.F. and X.F. conceived the project. Y.-F.F., P.H., and X.F. designed the experiments. Y.-F.F., X.F., P.H., X.Z., and Z.C. analyzed the results. P.H., X.Z., Z.C., X.W., Y.M., and G.H. performed all the experiments and analyzed the data. P.H. and Y.-F.F. created the figures. Y.-F.F. and P.H. wrote the manuscript. X.F., Y.-F.F., and Y.M. reviewed the manuscript.

Figure legends

Fig. 1. An intact Nup107–160 sub-complex is a prerequisite for its protein stability.

A to **D**, Immunoblots showing the level of endogenous Nup96 (**A**, anti-Nup96 antibody) and HOS1 (**B**, anti-HOS1 antibody) or Nup107-MYC (**C**, anti-MYC antibody) and HOS1-MYC (**D**, anti-MYC antibody) in nuclear extracts from wild-type plants and different mutants. Relative quantification of each band compared to the control is indicated below the bottom panel. **E**, Abundance of endogenous Nup96 (anti-Nup96 antibody) and HOS1 (anti-HOS1 antibody) proteins in nuclear extracts from the *nup98a-1 nup98b-1* and *nup98a-2 nup98b-1* double mutants. **F** to **I**, RT-qPCR analysis of endogenous *Nup96* (**F**) and *HOS1* (**G**) or transgenic *Nup107-MYC* (**H**) and *HOS1-MYC* (**I**) transcript levels. Seedlings were grown in long-day conditions for 10 days. Values are means ± standard deviation (SD; n = 3 biological repeats). Histone H3.1 (H3.1) was used as the loading control in immunoblots and relative quantification of each band compared to the control is indicated below the panel. *TIP41* was used as a reference gene for RT-qPCR. **J**, The nuclei in rosette leaves of wild-type and mutants were stained with Hoechst 33342 and were observed using a confocal laser scanning microscope. Scale bars, 20 μm. **Insets**, magnified images of nuclei. **K** and **L**, Major axis length (**K**) and circularity index (**L**) of nuclei, measured in wild-type plants and different mutants. Values are means ± SD (n ≥ 30). Different lowercase letters indicate significant differences (*, $P < 0.05$) using one-way ANOVA.

Fig. 2. Mutants of Y-complex components share similar transcriptome signatures and *FLC* chromatin histone modification profile.

A, Cluster dendrogram based on the differentially expressed genes in *hos1-3*, *nup96-1*, *nup160-3*, *nup107-3,* and *nup85-1* mutants compared to wild-type plants. **B**, Venn diagram of common and unique DEGs (An absolute Log2(FC) > 1, Fisher's exact test, *P*-value < 0.01) that are upregulated (left) or downregulated (right) in *hos1-3*, *nup96-1*, *nup160-3*, *nup107-3,* and *nup85-1* mutants compared to wild-type plants. **C**, Heatmap representation of mis-regulated flowering-related genes in *hos1-3*, *nup96-1*, *nup85-1*, *nup107-3,* and *nup160-3* mutants relative to wild-type plants. **D**, Relative *FLC* expression in Col-0 and different mutants. Values are means ± SD (n = 3 biological repeats). Different lowercase letters indicate significant differences (*, $P < 0.05$) using one-way ANOVA. **E** and **F**, Flowering phenotypes (**E**) of wild-type plants, *nup96-1*, *flc-3,* and *nup96-1 flc-3* mutants and total rosette leaf number (**F**) in long days. Values are means ± SD (n ≥ 18). **G**, RT-qPCR analysis of daily expression patterns of *FLC* in the *nup96-1* mutant and wild-type plants in long days. **H**, RT-qPCR analysis of developmental expression patterns of *Nup96* and *FLC* in wild-type seedlings in long days. Values are means ± SD (n = 3 biological repeats). **I**, Diagram of the *FLC* genomic region. P1 to P5 indicate the *FLC* chromatin regions examined by chromatin immunoprecipitation followed by quantitative PCR (ChIP-qPCR). The numbers below indicate nucleotide positions relative to the ATG start codon. Black boxes represent exons; lines indicate introns, and white boxes denote the untranslated regions. **J** to **L**, ChIP-qPCR assay of the relative enrichment levels of H3Ac (**J**), H3K4Me3 (**K**), H3K27Me3 (**L**) at the *FLC* locus in wild type and *hos1-3*, *nup96-1*, *nup107-3*, *nup160-3*, and *nup85-1* mutants. Seedlings were grown in long days for 10 days. Values are means ± SD (n = 3 biological repeats). The *eIF4A* gene was used for normalizing the quantified DNA fragments. Statistical analysis was performed using Student's *t* test (*, $P < 0.05$).

Fig. 3. Different Y-complex components interact with HOS1 to change histone modifications of *FLC* chromatin.

A, Yeast two-hybrid (Y2H) assay to detect interactions between HOS1 and Nup107–Nup160 sub-complex components. **B** to **D**, in vivo interaction of HOS1 with Nup96 (**B**), Nup160 (**C**), and Nup107 (**D**) in Arabidopsis. Plant total proteins extracted from 10-day transgenic seedlings grown in long days were immunoprecipitated with an anti-GFP antibody (**B** and **C**) or anti-MYC antibody (**D**) as indicated in each blot. The co-immunoprecipitated proteins were detected with anti-GFP, anti-MYC, or anti-HOS1 antibodies as indicated. **E**, Colocalization of Nup107-GFP and HOS1-mCherry in the roots of transgenic seedlings. Scale bars, 20 μm. **F**, Bimolecular fluorescence complementation (BiFC) assay showing HOS1 interacting with Nup107 in transgenic plants. HOS1 was fused to the C-terminal half of YFP (HOS1-YFPc), while Nup107 was fused to the N-terminal half of YFP (Nup107-YFPn). Scale bars, 10 μm. **G**, Flowering phenotypes of wild type, *nup96-1* and *hos1-3* single mutants, and the *nup96-1 hos1-3* double mutant grown in long-day conditions. **H**, Rosette leaf number at the time of flowering for the different genotypes shown in (**G**). Values are means ± SD (n ≥18). Statistical analysis was performed using Student's *t* test (*, $P < 0.05$). **I**, Relative *FLC* expression in wild-type, *nup96-1*, *hos1-3*, and *nup96-1 hos1-3* seedlings grown in long-day conditions. Values are means ± SD (n = 3 biological repeats). *TIP41* (At4g34270) was used as a reference gene. Statistical analysis was performed using Student's *t* test (*, $P < 0.05$). **J** to **L**, ChIP-qPCR analysis of relative enrichment levels of H3Ac (**J**), H3K4Me3 (**K**), H3K27Me3 (**L**) at the *FLC* locus in seedlings of wild type, *nup96-1* and the *hos1-3* single mutants and the *nup96-1 hos1-3* double mutant grown in long-day conditions for 10 days. Values are means ± SD (n = 3 biological repeats). The *eIF4A* gene was used for normalizing the quantified DNA fragments. Statistical analysis was performed using Student's *t* test (*, $P < 0.05$).

Fig. 4. Y-complex components associate with HDA6 to epigenetically modify histones over the *FLC* chromatin.

A, BiFC assay of HDA6-YFPc and Nup96-YFPn in the roots of transgenic seedlings. Scale bars, 20 μm. **B**, Subcellular distribution of HDA6-GFP in root epidermal cells of two *HDA6pro:HDA6-GFP* transgenic Arabidopsis seedlings (#1 and #2), showing high fluorescent signals at the nuclear rim. Scale bars, 20 μm. **C**, Immunoblotting on the purified nuclear envelope extracts of *HDA6pro:HDA6-GFP* transgenic lines compared to corresponding cytoplasm and nuclear samples and probed with the indicated antibodies. Nup96 was a positive control for the nuclear envelope fraction; histone H3.1 was a positive control for the nuclear fraction, and Actin was a positive control for the cytoplasmic fraction. **D**, In vivo interaction of Nup96 and HDA6 in *35S:HDA6-MYC* transgenic Arabidopsis lines. Cell extracts from 10-day-old seedlings were immunoprecipitated with an anti-MYC antibody. The precipitates were probed by immunoblotting with an anti-Nup96 antibody. **E** and **F** In vivo interaction of HDA6 with Nup107 (**E**), or Nup160 (**F**). Total proteins of *N. benthamiana* leaves co-expressing *HDA6-GFP* and *Nup107-MYC* (**E**) or *Nup160-MYC* (**F**) were immunoprecipitated with an anti-GFP antibody. The precipitates were probed by immunoblotting with an anti-MYC antibody. **G**, In vivo interaction assay of HDA6 with HOS1 and Nup96 in *35S:HDA6-MYC* transgenic lines. Cell extracts from 10-day-old seedlings were immunoprecipitated with an anti-MYC antibody. The precipitates were probed by immunoblotting with anti-Nup96 or anti-HOS1 antibodies. **H**, Immunoblotting analysis of HDA6-GFP in *HDA6pro:HDA6-GFP*, *hos1-3 HDA6pro:HDA6-GFP*, *nup96-1 HDA6pro:HDA6-GFP*, and *nup160-3 HDA6pro:HDA6-GFP* transgenic lines. **I**, ChIP-qPCR assay of relative enrichment levels of HDA6-GFP at the *FLC* locus in *HDA6pro:HDA6-GFP*, *hos1-3 HDA6pro:HDA6-GFP*, *nup96-1 HDA6pro:HDA6-GFP*, and *nup160-3 HDA6pro:HDA6-GFP* transgenic plants, using an anti-GFP antibody.

Fig. 5. Nup96 regulation of *FLC* chromatin modifications is associated with *FVE*.

A and **B**, Flowering phenotypes (**A**) and total rosette leaf number (**B**) of wild-type plants, *nup96-1* and *fve-3* single mutants, and the *nup96-1 fve-3* double mutant in long days. Values in (B) are means ± SD (n ≥ 18). **C**, Relative *FLC* expression in mutants and wild-type plants. Values are means ± SD (n = 3 biological repeats). **D** to **F**, ChIP-qPCR analysis of relative enrichment levels for H3Ac (**D**), H3K4Me3 (**E**), and H3K27Me3 (**F**) at the *FLC* locus in wild type, *nup96-1*, *fve-3*, and *nup96- fve-3*. Seedlings were grown in long-day conditions for 10 days. Values are means ± SD (n = 3 biological repeats). The *eIF4A* gene was used for normalizing the quantified DNA fragments while *TIP41* was used as a reference gene for RT-qPCR. Different lowercase letters indicate significant differences (*, $P < 0.05$) using one-way ANOVA.

Fig. 6 The Y-complex is intimately associated with histone H2A proteins at the nuclear envelope.

A to **C**, BiFC assay of HTA6 **(A)**, HTA9 **(B)**, and HTA13 **(C)** interacting with different Y-complex components in *N. benthamiana.* HTAs were fused to the C-terminal half of YFP (HTA6-YFPc, HTA9-YFPc, HTA13-YFPc), while Y-complex components were fused to the N-terminal half of YFP (HOS1-YFPn, Nup96-YFPn, Nup107-YFPn). SUN1 (an inner nuclear membrane protein) served as negative control. mRFP-AHL22 served as a marker for nuclear localization. Scale bars, 10 μm. **D**, Left, BiFC assay of HTA6, HTA9, and HTA13 interacting with Nup96-TMD in *N. benthamiana*. mRFP-AHL22, served as a marker for nuclear localization. Right, measurement of YFP fluorescence intensity profiles along the lines indicated to the left. The peaks indicated by the red arrows represent the nuclear membrane positioning signal. Scale bars, 10 μm. **E** to **G**, In vivo interaction of HTA9 with HOS1 (**E**), Nup96 (**F**), and Nup107 (**G**) in Arabidopsis. Plant total proteins extracted from 10-day-old

seedlings grown in long days were immunoprecipitated with an anti-HTA9 antibody. The co-immunoprecipitated proteins were probed with anti-HOS1 or anti-MYC antibody as indicated on the blots. **H** and **I**, Immunoblots showing the level of endogenous H2A (**H**) or HTA9 (**I**) in nuclear extracts from wild-type plants and different mutants. Histone H3.1 (H3.1) was used as the loading control.

Fig. 7. The Nup107–Nup160 sub-complex regulates the position of the *FLC* locus in the nucleus.

A and **B**, ChIP-qPCR assay of the relative enrichment levels of Nup96, HOS1, and Nup107 proteins at the *FLC* locus in different transgenic plants with anti-GFP (**A**) or anti-MYC (**B**) antibodies. Seedlings were grown in long days for 10 days. **C** and **D**, In vivo interaction of RPBII with HOS1 (**C**) and Nup107 (**D**) in Arabidopsis. Plant total proteins extracted from 10-day seedlings grown in long days were immunoprecipitated by anti-RPBII antibodies. The co-immunoprecipitated proteins were probed with anti-HOS1, anti-MYC, or anti-Ubiquitin antibodies as indicated on the blots. **E**, Immunoblots showing the level of endogenous RPBII in nuclear extracts from wild-type plants and different mutants. Histone H3.1 (H3.1) was used as the loading control. **F**, ChIP-qPCR assay of the relative enrichment levels of RNA Pol II at the *FLC* locus in wild type, *hos1-3*, *nup96-1*, *nup160-3* and *hos1-3 nup96-1*. Seedlings were grown in long days for 10 days. **G**, Visualization of the *FLC* locus in the nucleus of wild type and *nup96-1* by fluorescence in situ hybridization (FISH). FISH signals are shown in red (white arrows); the nuclei were counterstained with DAPI (blue). Scale bars, 2 μm. **H** and **I**, Distribution of the *FLC* locus and average percentage of *FLC* locus localizing to the nuclear peripheral zone in wild type (**H**) and *nup96-1* (**I**). The red bars in the histogram represent the nuclear peripheral zone—the region from 0 μm to 0.2 μm from the nuclear edge. The average percentage of *FLC* loci within the nuclear peripheral zone with standard error (SE) from three independent replicates is shown. “n”

represents the total number of FISH signals analyzed from all replicates. The *FLC* distribution data from the wild type was compared to that of *nup96-1* using a two-sided *t*-test, (*, $P < 0.05$).

Fig. 8. A model for Y-complex function as a platform for *FLC* epigenetic modification conferring flowering regulation.

In wild-type plants, the intact Y-complex recruits *FLC* chromatin to the nuclear pore complex via interaction with histone proteins, and then facilitating RNA Pol II to be enriched on the chromatin and resulting in *FLC* expression. In Y-complex mutants, the recruitment of *FLC* chromatin is disrupted and the histone modification pattern is changed, leading to inhibition of *FLC* expression and early flowering.

References

Agote-Aran, A., Schmucker, S., Jerabkova, K., Jmel Boyer, I., Berto, A., Pacini, L., Ronchi, P., Kleiss, C., Guerard, L., Schwab, Y., Moine, H., Mandel, J.L., Jacquemont, S., Bagni, C., and Sumara, I. (2020). Spatial control of nucleoporin condensation by fragile X-related proteins. EMBO J **39,** e104467.

Allen, J.L., and Douglas, M.G. (1989). Organization of the nuclear pore complex in Saccharomyces cerevisiae. J Ultra struct Mol Struct Res **102,** 95-108.

Ausin, I., Alonso-Blanco, C., Jarillo, J.A., Ruiz-Garcia, L., and Martinez-Zapater, J.M. (2004). Regulation of flowering time by FVE, a retinoblastoma-associated protein. Nat Genet **36,** 162-166.

Bastow, R., Mylne, J.S., Lister, C., Lippman, Z., Martienssen, R.A., and Dean, C. (2004). Vernalization requires epigenetic silencing of FLC by histone methylation. Nature **427,** 164-167.

Berry, S., and Dean, C. (2015). Environmental perception and epigenetic memory: mechanistic insight through FLC. Plant J **83,** 133-148.

Bouche, F., Lobet, G., Tocquin, P., and Perilleux, C. (2016). FLOR-ID: an interactive database of flowering-time gene networks in Arabidopsis thaliana. Nucleic Acids Res **44,** D1167-D1171.

Cao, Y., Dai, Y., Cui, S., and Ma, L. (2008). Histone H2B monoubiquitination in the chromatin of FLOWERING LOCUS C regulates flowering time in Arabidopsis. Plant Cell **20,** 2586-2602.

Chakraborty, P., Wang, Y., Wei, J.H., van Deursen, J., Yu, H., Malureanu, L., Dasso, M., Forbes, D.J., Levy, D.E., Seemann, J., and Fontoura, B.M. (2008). Nucleoporin

levels regulate cell cycle progression and phase-specific gene expression. Dev Cell **15,** 657-667.

Chen, Q.J., Zhou, H.M., Chen, J., and Wang, X.C. (2006). Using a modified TA cloning method to create entry clones. Anal Biochem **358,** 120-125.

Cheng, Z., Zhang, X., Huang, P., Huang, G., Zhu, J., Chen, F., Miao, Y., Liu, L., Fu, Y.F., and Wang, X. (2020). Nup96 and HOS1 Are Mutually Stabilized and Gate CONSTANS Protein Level, Conferring Long-Day Photoperiodic Flowering Regulation in Arabidopsis. Plant Cell **32,** 374-391.

Chow, K.H., Elgort, S., Dasso, M., Powers, M.A., and Ullman, K.S. (2014). The SUMO proteases SENP1 and SENP2 play a critical role in nucleoporin homeostasis and nuclear pore complex function. Mol Biol Cell **25,** 160-168.

Chytilova, E., Macas, J., Sliwinska, E., Rafelski, S.M., Lambert, G.M., and Galbraith, D.W. (2000). Nuclear dynamics in Arabidopsis thaliana. Mol Biol Cell **11**, 2733-2741.

D'Angelo, M.A. (2018). Nuclear pore complexes as hubs for gene regulation. Nucleus-Phila **9,** 142-148.

Deal, R.B., Topp, C.N., McKinney, E.C., and Meagher, R.B. (2007). Repression of flowering in Arabidopsis requires activation of FLOWERING LOCUS C expression by the histone variant H2A.Z. Plant Cell **19,** 74-83.

Dechat, T., Pfleghaar, K., Sengupta, K., Shimi, T., Shumaker, D.K., Solimando, L., and Goldman, R.D. (2008). Nuclear lamins: major factors in the structural organization and function of the nucleus and chromatin. Genes Dev **22,** 832-853.

DeGrasse, J.A., DuBois, K.N., Devos, D., Siegel, T.N., Sali, A., Field, M.C., Rout, M.P., and Chait, B.T. (2009). Evidence for a Shared Nuclear Pore Complex Architecture That Is Conserved from the Last Common Eukaryotic Ancestor. Mol Cell Proteomics **8,** 2119-2130.

Demmerle, J., Koch, A.J., and Holaska, J.M. (2013). Emerin and histone deacetylase 3 (HDAC3) cooperatively regulate expression and nuclear positions of MyoD, Myf5, and Pax7 genes during myogenesis. Chromosome Res **21,** 765-779.

Dittmer, T.A., Stacey, N.J., Sugimoto-Shirasu, K., and Richards, E.J. (2007). LITTLE NUCLEI genes affecting nuclear morphology in Arabidopsis thaliana. Plant Cell **19,** 2793-2803.

Earley, K.W., Haag, J.R., Pontes, O., Opper, K., Juehne, T., Song, K.M., and Pikaard, C.S. (2006). Gateway-compatible vectors for plant functional genomics and proteomics. Plant J **45,** 616-629.

Feng, C.M., Qiu, Y.J., Van Buskirk, E.K., Yang, E.J., and Chen, M. (2014). Light-regulated gene repositioning in Arabidopsis. Nat Commun **5**.

Fiserova, J., Kiseleva, E., and Goldberg, M.W. (2009). Nuclear envelope and nuclear pore complex structure and organization in tobacco BY-2 cells. Plant J **59,** 243-255.

Gall, J.G. (1967). Octagonal nuclear pores. J Cell Biol **32,** 391-399.

Gao, N., Davuluri, G., Gong, W.L., Seiler, C., Lorent, K., Furth, E.E., Kaestner, K.H., and Pack, M. (2011). The Nuclear Pore Complex Protein Elys Is Required for Genome Stability in Mouse Intestinal Epithelial Progenitor Cells. Gastroenterology **140,** 1547-U1252.

Gao, X., Yu, S., Guan, Y., Shen, Y., and Xu, L. (2021). Nucleoporin 50 mediates Kcna4

transcription to regulate cardiac electrical activity. J Cell Sci **134**.

Geli, V., and Lisby, M. (2015). Recombinational DNA repair is regulated by compartmentalization of DNA lesions at the nuclear pore complex. Bioessays **37,** 1287-1292.

Goldberg, M.W., and Allen, T.D. (1996). The nuclear pore complex and lamina: three-dimensional structures and interactions determined by field emission in-lens scanning electron microscopy. J Mol Biol **257,** 848-865.

Goto, C., Hara-Nishimura, I., and Tamura, K. (2021). Regulation and Physiological Significance of the Nuclear Shape in Plants. Frontiers in plant science **12,** 673905.

Gozalo, A., Duke, A., Lan, Y., Pascual-Garcia, P., Talamas, J.A., Nguyen, S.C., Shah, P.P., Jain, R., Joyce, E.F., and Capelson, M. (2020). Core Components of the Nuclear Pore Bind Distinct States of Chromatin and Contribute to Polycomb Repression. Mol Cell **77,** 67-81 e67.

Griffis, E.R., Xu, S., and Powers, M.A. (2003). Nup98 localizes to both nuclear and cytoplasmic sides of the nuclear pore and binds to two distinct nucleoporin subcomplexes. Mol Biol Cell **14,** 600-610.

Groves, N.R., McKenna, J.F., Evans, D.E., Graumann, K., and Meier, I. (2019). A nuclear localization signal targets tail-anchored membrane proteins to the inner nuclear envelope in plants. J Cell Sci **132**.

Gu, X., Jiang, D., Yang, W., Jacob, Y., Michaels, S.D., and He, Y. (2011a). Arabidopsis homologs of retinoblastoma-associated protein 46/48 associate with a histone deacetylase to act redundantly in chromatin silencing. PLoS genetics **7,** e1002366.

Gu, X.F., Jiang, D.H., Yang, W.N., Jacob, Y., Michaels, S.D., and He, Y.H. (2011b). Arabidopsis Homologs of Retinoblastoma-Associated Protein 46/48 Associate with a Histone Deacetylase to Act Redundantly in Chromatin Silencing. Plos Genet **7**.

Gu, Y. (2018). The nuclear pore complex: a strategic platform for regulating cell signaling. New Phytol **219,** 25-30.

Gutierrez, L., Mauriat, M., Guenin, S., Pelloux, J., Lefebvre, J.F., Louvet, R., Rusterucci, C., Moritz, T., Guerineau, F., Bellini, C., and Van Wuytswinkel, O. (2008). The lack of a systematic validation of reference genes: a serious pitfall undervalued in reverse transcription-polymerase chain reaction (RT-PCR) analysis in plants. Plant Biotechnol J **6,** 609-618.

Hayama, R., Sarid-Krebs, L., Richter, R., Fernandez, V., Jang, S., and Coupland, G. (2017). PSEUDO RESPONSE REGULATORs stabilize CONSTANS protein to promote flowering in response to day length. Embo J **36,** 904-918.

He, Y., Michaels, S.D., and Amasino, R.M. (2003). Regulation of flowering time by histone acetylation in Arabidopsis. Science **302,** 1751-1754.

He, Y., Doyle, M.R., and Amasino, R.M. (2004). PAF1-complex-mediated histone methylation of FLOWERING LOCUS C chromatin is required for the vernalization-responsive, winter-annual habit in Arabidopsis. Genes Dev **18,** 2774-2784.

Hepworth, J., and Dean, C. (2015). Flowering Locus C's Lessons: Conserved Chromatin Switches Underpinning Developmental Timing and Adaptation. Plant Physiol **168,** 1237-1245.

Huang, X., Zhang, Q., Jiang, Y.P., Yang, C.W., Wang, Q.Y., and Li, L. (2018). Shade-

induced nuclear localization of PIF7 is regulated by phosphorylation and 14-3-3 proteins in Arabidopsis. Elife **7**.

Ibarra, A., and Hetzer, M.W. (2015). Nuclear pore proteins and the control of genome functions. Genes Dev **29,** 337-349.

Jacinto, F.V., Benner, C., and Hetzer, M.W. (2015). The nucleoporin Nup153 regulates embryonic stem cell pluripotency through gene silencing. Gene Dev **29,** 1224-1238.

Jacob, Y., Mongkolsiriwatana, C., Veley, K.M., Kim, S.Y., and Michaels, S.D. (2007). The nuclear pore protein AtTPR is required for RNA homeostasis, flowering time, and auxin signaling. Plant Physiol **144,** 1383-1390.

Jeon, J., and Kim, J. (2011). FVE, an Arabidopsis Homologue of the Retinoblastoma-Associated Protein That Regulates Flowering Time and Cold Response, Binds to Chromatin as a Large Multiprotein Complex. Mol Cells **32,** 227-234.

Jiang, S., Xiao, L., Huang, P., Cheng, Z., Chen, F., Miao, Y., Fu, Y.F., Chen, Q., and Zhang, X.M. (2019). Nucleoporin Nup98 participates in flowering regulation in a CONSTANS-independent mode. Plant Cell Rep **38,** 1263-1271.

Jung, H., Yan, J., Zhai, Z., and Vatamaniuk, O.K. (2015). Gene functional analysis using protoplast transient assays. Methods Mol Biol **1284,** 433-452.

Jung, J.H., Park, J.H., Lee, S., To, T.K., Kim, J.M., Seki, M., and Park, C.M. (2013). The cold signaling attenuator HIGH EXPRESSION OF OSMOTICALLY RESPONSIVE GENE1 activates FLOWERING LOCUS C transcription via chromatin remodeling under short-term cold stress in Arabidopsis. Plant Cell **25,** 4378-4390.

Kim, J.M., To, T.K., and Seki, M. (2012). An epigenetic integrator: new insights into genome regulation, environmental stress responses and developmental controls by histone deacetylase 6. Plant Cell Physiol **53,** 794-800.

Koornneef, M., Hanhart, C.J., and van der Veen, J.H. (1991). A genetic and physiological analysis of late flowering mutants in Arabidopsis thaliana. Mol Gen Genet **229,** 57-66.

Koornneef, M., Alonso-Blanco, C., Blankestijn-de Vries, H., Hanhart, C.J., and Peeters, A.J.M. (1998). Genetic interactions among late-flowering mutants of Arabidopsis. Genetics **148,** 885-892.

Kosak, S.T., Skok, J.A., Medina, K.L., Riblet, R., Le Beau, M.M., Fisher, A.G., and Singh, H. (2002). Subnuclear compartmentalization of immunoglobulin loci during lymphocyte development. Science **296,** 158-162.

Kuhn, T.M., and Capelson, M. (2019). Nuclear Pore Proteins in Regulation of Chromatin State. Cells-Basel **8**.

Lee, H., Xiong, L., Gong, Z., Ishitani, M., Stevenson, B., and Zhu, J.K. (2001). The Arabidopsis HOS1 gene negatively regulates cold signal transduction and encodes a RING finger protein that displays cold-regulated nucleo--cytoplasmic partitioning. Genes Dev **15,** 912-924.

Lee, J.H., Yoo, S.J., Park, S.H., Hwang, I., Lee, J.S., and Ahn, J.H. (2007). Role of SVP in the control of flowering time by ambient temperature in Arabidopsis. Genes Dev **21,** 397-402.

Lee, J.H., Kim, J.J., Kim, S.H., Cho, H.J., Kim, J., and Ahn, J.H. (2012). The E3 ubiquitin ligase HOS1 regulates low ambient temperature-responsive flowering in Arabidopsis thaliana. Plant Cell Physiol **53,** 1802-1814.

Lei, B.K., and Berger, F. (2020). H2A Variants in Arabidopsis: Versatile Regulators of Genome Activity. Plant Communications **1**.

Li, C., Liu, L., Teo, Z.W.N., Shen, L., and Yu, H. (2020). Nucleoporin 160 Regulates Flowering through Anchoring HOS1 for Destabilizing CO in Arabidopsis. Plant Commun **1,** 100033.

Li, D., Liu, C., Shen, L., Wu, Y., Chen, H., Robertson, M., Helliwell, C.A., Ito, T., Meyerowitz, E., and Yu, H. (2008). A repressor complex governs the integration of flowering signals in Arabidopsis. Dev Cell **15,** 110-120.

Li, X., and Gu, Y.N. (2020). Structural and functional insight into the nuclear pore complex and nuclear transport receptors in plant stress signaling. Current Opinion in Plant Biology **58,** 60-68.

Lin, D.H., and Hoelz, A. (2019). The Structure of the Nuclear Pore Complex (An Update). Annu Rev Biochem **88,** 725-783.

Liu, F., Quesada, V., Crevillen, P., Baurle, I., Swiezewski, S., and Dean, C. (2007). The Arabidopsis RNA-binding protein FCA requires a lysine-specific demethylase 1 homolog to downregulate FLC. Mol Cell **28,** 398-407.

Liu, X., Luo, M., and Wu, K. (2012a). Epigenetic interplay of histone modifications and DNA methylation mediated by HDA6. Plant signaling & behavior **7,** 633-635.

Liu, X.C., Yu, C.W., Duan, J., Luo, M., Wang, K.C., Tian, G., Cui, Y.H., and Wu, K.Q. (2012b). HDA6 Directly Interacts with DNA Methyltransferase MET1 and Maintains Transposable Element Silencing in Arabidopsis. Plant Physiology **158,** 119-129.

Liu, Z.X., Yan, M.B., Liang, Y.J., Liu, M., Zhang, K., Shao, D.D., Jiang, R.C., Li, L., Wang, C.M., Nussenzveig, D.R., Zhang, K.K., Chen, S.X., Zhong, C.Q., Mo, W., Fontoura, B.M.A., and Zhang, L. (2019). Nucleoporin Seh1 Interacts with Olig2/Brd7 to Promote Oligodendrocyte Differentiation and Myelination. Neuron **102,** 587-+.

Loiodice, I., Alves, A., Rabut, G., Van Overbeek, M., Ellenberg, J., Sibarita, J.B., and Doye, V. (2004). The entire Nup107-160 complex, including three new members, is targeted as one entity to kinetochores in mitosis. Mol Biol Cell **15,** 3333-3344.

Meier, I., Richards, E.J., and Evans, D.E. (2017). Cell Biology of the Plant Nucleus. Annu Rev Plant Biol **68,** 139-172.

Meister, P., Towbin, B.D., Pike, B.L., Ponti, A., and Gasser, S.M. (2010). The spatial dynamics of tissue-specific promoters during C-elegans development. Gene Dev **24,** 766-782.

Michaels, S.D., and Amasino, R.M. (1999). FLOWERING LOCUS C encodes a novel MADS domain protein that acts as a repressor of flowering. Plant Cell **11,** 949-956.

Morchoisne-Bolhy, S., Geoffroy, M.C., Bouhlel, I.B., Alves, A., Auduge, N., Baudin, X., Van Bortle, K., Powers, M.A., and Doye, V. (2015). Intranuclear dynamics of the Nup107-160 complex. Mol Biol Cell **26,** 2343-2356.

Niu, Y.X., Bai, J.T., Liu, X.Y., Zhang, H., Bao, J.P., Zhao, W.S., Hou, Y.F., Deng, X., Yang, C., Guo, L., Geng, Z.Y., Xie, H.L., Wu, H.Y., Shen, M., Lou, X.J., Tang, W.Q., Liu, X.G., Sun, D.Y., Cao, X.F., and Zheng, S.Z. (2022). HISTONE DEACETYLASE 9 transduces heat signal in plant cells. P Natl Acad Sci USA **119**.

Parry, G. (2014). Components of the Arabidopsis nuclear pore complex play multiple diverse roles in control of plant growth. J Exp Bot **65,** 6057-6067.

Parry, G., Ward, S., Cernac, A., Dharmasiri, S., and Estelle, M. (2006). The Arabidopsis SUPPRESSOR OF AUXIN RESISTANCE proteins are nucleoporins with an important role in hormone signaling and development. Plant Cell **18,** 1590-1603.

Ptak, C., and Wozniak, R.W. (2016). Nucleoporins and chromatin metabolism. Curr Opin Cell Biol **40,** 153-160.

Ragoczy, T., Bender, M.A., Telling, A., Byron, R., and Groudine, M. (2006). The locus control region is required for association of the murine beta-globin locus with engaged transcription factories during erythroid maturation. Gene Dev **20,** 1447-1457.

Rajoo, S., Vallotton, P., Onischenko, E., and Weis, K. (2018). Stoichiometry and compositional plasticity of the yeast nuclear pore complex revealed by quantitative fluorescence microscopy. Proc Natl Acad Sci U S A **115,** E3969-E3977.

Rosa, S., Duncan, S., and Dean, C. (2016). Mutually exclusive sense-antisense transcription at FLC facilitates environmentally induced gene repression. Nat Commun **7,** 13031.

Rosa, S., De Lucia, F., Mylne, J.S., Zhu, D., Ohmido, N., Pendle, A., Kato, N., Shaw, P., and Dean, C. (2013). Physical clustering of FLC alleles during Polycomb-mediated epigenetic silencing in vernalization. Gene Dev **27,** 1845-1850.

Sakamoto, Y., Sato, M., Sato, Y., Harada, A., Suzuki, T., Goto, C., Tamura, K., Toyooka, K., Kimura, H., Ohkawa, Y., Hara-Nishimura, I., Takagi, S., and Matsunaga, S. (2020). Subnuclear gene positioning through lamina association affects copper tolerance. Nature communications **11,** 5914.

Salas-Pino, S., Gallardo, P., Barrales, R.R., Braun, S., and Daga, R.R. (2017). The fission yeast nucleoporin Alm1 is required for proteasomal degradation of kinetochore components. Journal of Cell Biology **216,** 3591-3608.

Saleh, A., Alvarez-Venegas, R., and Avramova, Z. (2008). An efficient chromatin immunoprecipitation (ChIP) protocol for studying histone modifications in Arabidopsis plants. Nat Protoc **3,** 1018-1025.

Seo, E., Lee, H., Jeon, J., Park, H., Kim, J., Noh, Y.S., and Lee, I. (2009). Crosstalk between Cold Response and Flowering in Arabidopsis Is Mediated through the Flowering-Time Gene SOC1 and Its Upstream Negative Regulator FLC. Plant Cell **21,** 3185-3197.

Simpson, G.G. (2004). The autonomous pathway: epigenetic and post-transcriptional gene regulation in the control of Arabidopsis flowering time. Curr Opin Plant Biol **7,** 570-574.

Smith, S., Galinha, C., Desset, S., Tolmie, F., Evans, D., Tatout, C., and Graumann, K. (2015). Marker gene tethering by nucleoporins affects gene expression in plants. Nucleus **6,** 471-478.

Sura, W., Kabza, M., Karlowski, W.M., Bieluszewski, T., Kus-Slowinska, M., Paweloszek, L., Sadowski, J., and Ziolkowski, P.A. (2017). Dual Role of the Histone Variant H2A.Z in Transcriptional Regulation of Stress-Response Genes. Plant Cell **29,** 791-807.

Talbert, P.B., and Henikoff, S. (2010). Histone variants - ancient wrap artists of the epigenome. Nat Rev Mol Cell Bio **11,** 264-275.

Tamura, K. (2020). Nuclear pore complex-mediated gene expression in Arabidopsis thaliana. J Plant Res **133,** 449-455.

Tamura, K., and Hara-Nishimura, I. (2011). Involvement of the nuclear pore complex in morphology of the plant nucleus. Nucleus-Phila **2,** 168-172.

Tamura, K., Fukao, Y., Iwamoto, M., Haraguchi, T., and Hara-Nishimura, I. (2010). Identification and characterization of nuclear pore complex components in Arabidopsis thaliana. Plant Cell **22,** 4084-4097.

Tang, Y., Dong, Q., Wang, T., Gong, L., and Gu, Y. (2021). PNET2 is a component of the plant nuclear lamina and is required for proper genome organization and activity. Dev Cell.

Vaquerizas, J.M., Suyama, R., Kind, J., Miura, K., Luscombe, N.M., and Akhtar, A. (2010). Nuclear pore proteins nup153 and megator define transcriptionally active regions in the Drosophila genome. PLoS genetics **6,** e1000846.

Walther, T.C., Alves, A., Pickersgill, H., Loiodice, I., Hetzer, M., Galy, V., Hulsmann, B.B., Kocher, T., Wilm, M., Allen, T., Mattaj, I.W., and Doye, V. (2003). The conserved Nup107-160 complex is critical for nuclear pore complex assembly. Cell **113,** 195-206.

Wang, X., Fan, C.M., Zhang, X.M., Zhu, J.L., and Fu, Y.F. (2013). BioVector, a flexible system for gene specific-expression in plants. Bmc Plant Biol **13**.

Whittaker, C., and Dean, C. (2017). The FLC Locus: A Platform for Discoveries in Epigenetics and Adaptation. Annu Rev Cell Dev Biol **33,** 555-575.

Wong, R.W., Mamede, J.I., and Hope, T.J. (2015). Impact of Nucleoporin-Mediated Chromatin Localization and Nuclear Architecture on HIV Integration Site Selection. J Virol **89,** 9702-9705.

Wong, X., Melendez-Perez, A.J., and Reddy, K.L. (2022). The Nuclear Lamina. Cold Spring Harbor perspectives in biology **14,** a040113.

Wu, K., Zhang, L., Zhou, C., Yu, C.W., and Chaikam, V. (2008). HDA6 is required for jasmonate response, senescence and flowering in Arabidopsis. J Exp Bot **59,** 225-234.

Wu, X.S., Kasper, L.H., Mantcheva, R.T., Mantchev, G.T., Springett, M.J., and van Deursen, J.M.A. (2001). Disruption of the FG nucleoporin NUP98 causes selective changes in nuclear pore complex stoichiometry and function. P Natl Acad Sci USA **98,** 3191-3196.

Wu, Z., Fang, X.F., Zhu, D.L., and Deati, C. (2020). Autonomous Pathway: FLOWERING LOCUS C Repression through an Antisense-Mediated Chromatin-Silencing Mechanism. Plant Physiology **182,** 27-37.

Xiao, L., Liu, W., Chen, F., Zhang, X., Chen, Q., and Fu, Y.-F. (2016). The Phenotype Analysis of NUP107-160 Subcomplex Mutants in Arabidopsis. J. Agri. Sci. Tech. **18,** 54-61.

Xiao, L., Jiang, S., Huang, P., Chen, F., Wang, X., Cheng, Z., Miao, Y., Liu, L., Searle, I., Liu, C., Wu, X.X., Fu, Y.F., Chen, Q., and Zhang, X.M. (2020). Two Nucleoporin98 homologous genes jointly participate in the regulation of starch degradation to repress senescence in Arabidopsis. Bmc Plant Biol **20,** 292.

Xu, X.M., Rose, A., Muthuswamy, S., Jeong, S.Y., Venkatakrishnan, S., Zhao, Q., and Meier, I. (2007). NUCLEAR PORE ANCHOR, the Arabidopsis homolog of Tpr/Mlp1/Mlp2/megator, is involved in mRNA export and SUMO homeostasis and

affects diverse aspects of plant development. Plant Cell **19,** 1537-1548.

Yang, H.C., Howard, M., and Dean, C. (2014). Antagonistic Roles for H3K36me3 and H3K27me3 in the Cold-Induced Epigenetic Switch at Arabidopsis FLC. Current Biology **24,** 1793-1797.

Yu, C.W., Chang, K.Y., and Wu, K.Q. (2016). Genome-Wide Analysis of Gene Regulatory Networks of the FVE-HDA6-FLD Complex in Arabidopsis. Frontiers in plant science **7**.

Yu, C.W., Liu, X., Luo, M., Chen, C., Lin, X., Tian, G., Lu, Q., Cui, Y., and Wu, K. (2011). HISTONE DEACETYLASE6 interacts with FLOWERING LOCUS D and regulates flowering in Arabidopsis. Plant Physiol **156,** 173-184.

Yu, X., and Michaels, S.D. (2010). The Arabidopsis Paf1c complex component CDC73 participates in the modification of FLOWERING LOCUS C chromatin. Plant Physiol **153,** 1074-1084.

Zhang, Y., and Li, X. (2005). A putative nucleoporin 96 Is required for both basal defense and constitutive resistance responses mediated by suppressor of npr1-1,constitutive 1. Plant Cell **17,** 1306-1316.

Zhao, Z., Yu, Y., Meyer, D., Wu, C., and Shen, W.H. (2005). Prevention of early flowering by expression of FLOWERING LOCUS C requires methylation of histone H3 K36. Nature cell biology **7,** 1256-1260.

Zhou, X., Graumann, K., Evans, D.E., and Meier, I. (2012). Novel plant SUN-KASH bridges are involved in RanGAP anchoring and nuclear shape determination. J Cell Biol **196,** 203-211.

Zhu, Y., Wang, B., Tang, K., Hsu, C.C., Xie, S., Du, H., Yang, Y., Tao, W.A., and Zhu, J.K. (2017). An Arabidopsis Nucleoporin NUP85 modulates plant responses to ABA and salt stress. PLoS genetics **13,** e1007124.

Zilberman, D., Coleman-Derr, D., Ballinger, T., and Henikoff, S. (2008). Histone H2A.Z and DNA methylation are mutually antagonistic chromatin marks. Nature **456,** 125-U114.

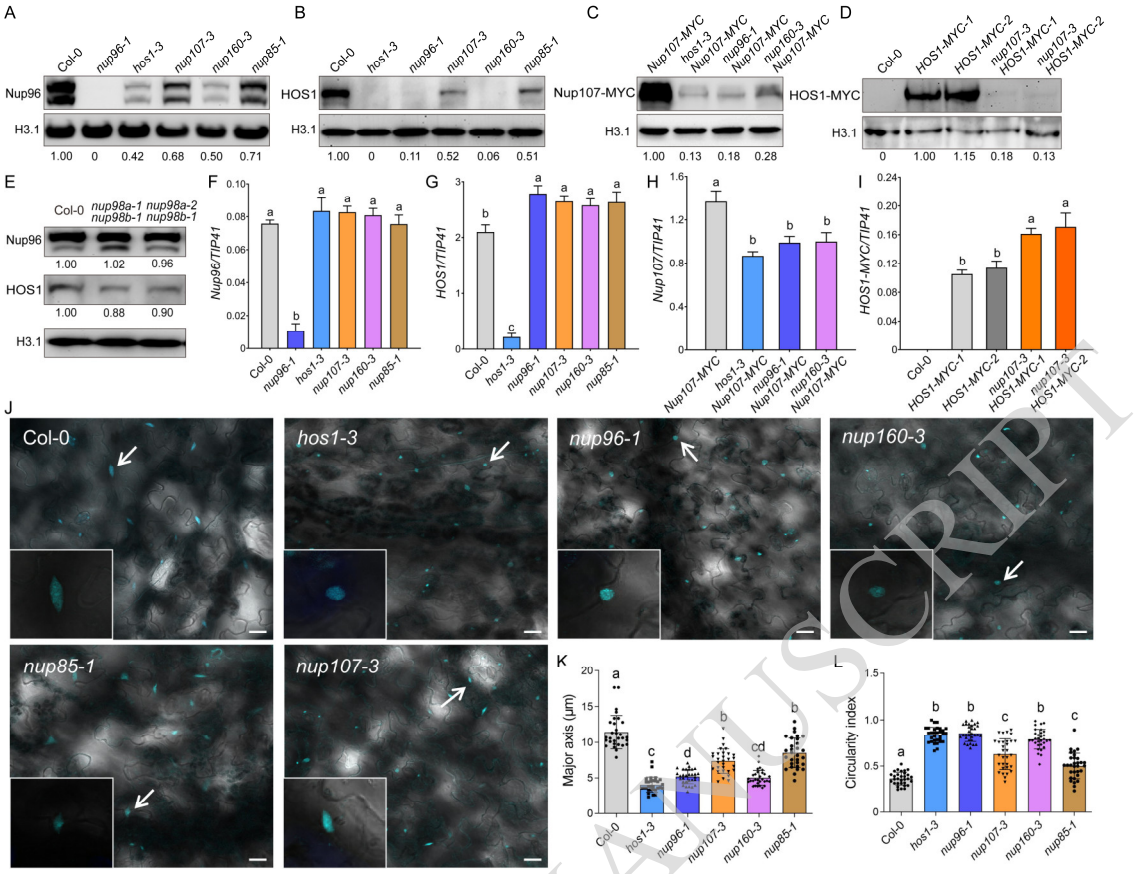

Fig. 1. An intact Nup107–160 sub-complex is a prerequisite for its protein stability.

A to **D**, Immunoblots showing the level of endogenous Nup96 (**A**, anti-Nup96 antibody) and HOS1 (**B**, anti-HOS1 antibody) or Nup107-MYC (**C**, anti-MYC antibody) and HOS1-MYC (**D**, anti-MYC antibody) in nuclear extracts from wild-type plants and different mutants. Relative quantification of each band compared to the control is indicated below the bottom panel. **E**, Abundance of endogenous Nup96 (anti-Nup96 antibody) and HOS1 (anti-HOS1 antibody) proteins in nuclear extracts from the *nup98a-1 nup98b-1* and *nup98a-2 nup98b-1* double mutants. **F** to **I**, RT-qPCR analysis of endogenous *Nup96* (**F**) and *HOS1* (**G**) or transgenic *Nup107-MYC* (**H**) and *HOS1-MYC* (**I**) transcript levels. Seedlings were grown in long-day conditions for 10 days. Values are means ± standard deviation (SD; n = 3 biological repeats). Histone H3.1 (H3.1) was used as the loading control in immunoblots and relative quantification of each band compared to the control is indicated below the panel. *TIP41* was used as a reference gene for RT-qPCR. **J**, The nuclei in rosette leaves of wild-type and mutants were stained with Hoechst 33342 and were observed using a confocal laser scanning microscope. Scale bars, 20 μm. **Insets**, magnified images of nuclei. **K** and **L**, Major axis length (**K**) and circularity index (**L**) of nuclei, measured in wild-type plants and different mutants. Values are means ± SD (n ≥ 30). Different lowercase letters indicate significant differences (*, $P < 0.05$) using one-way ANOVA.

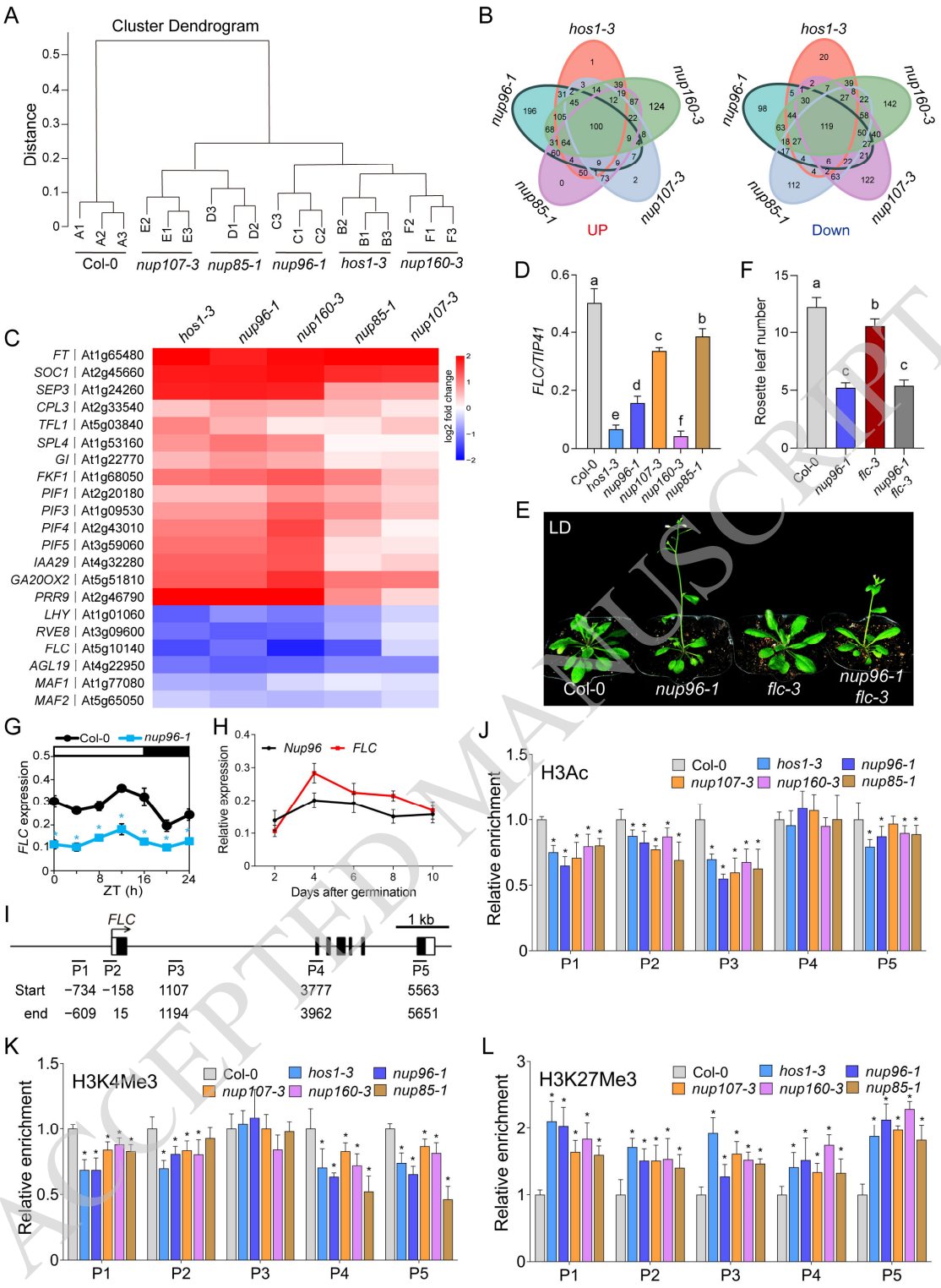

Fig. 2. Mutants of Y-complex components share similar transcriptome signatures and *FLC* chromatin histone modification profile.

A, Cluster dendrogram based on the differentially expressed genes in *hos1-3*, *nup96-1*, *nup160-3*, *nup107-3,* and *nup85-1* mutants compared to wild-type plants. **B**, Venn diagram of common and unique DEGs (An absolute Log2(FC) > 1, Fisher's exact test, *P*-value < 0.01) that are upregulated (left) or downregulated (right) in *hos1-3*, *nup96-1*, *nup160-3*, *nup107-3,* and *nup85-1* mutants compared to wild-type plants. **C**, Heatmap representation of mis-

regulated flowering-related genes in *hos1-3*, *nup96-1*, *nup85-1*, *nup107-3,* and *nup160-3* mutants relative to wild-type plants. **D**, Relative *FLC* expression in Col-0 and different mutants. Values are means ± SD (n = 3 biological repeats). Different lowercase letters indicate significant differences (*, $P < 0.05$) using one-way ANOVA. **E** and **F**, Flowering phenotypes (**E**) of wild-type plants, *nup96-1*, *flc-3,* and *nup96-1 flc-3* mutants and total rosette leaf number (**F**) in long days. Values are means ± SD (n ≥ 18). **G**, RT-qPCR analysis of daily expression patterns of *FLC* in the *nup96-1* mutant and wild-type plants in long days. **H**, RT-qPCR analysis of developmental expression patterns of *Nup96* and *FLC* in wild-type seedlings in long days. Values are means ± SD (n = 3 biological repeats). **I**, Diagram of the *FLC* genomic region. P1 to P5 indicate the *FLC* chromatin regions examined by chromatin immunoprecipitation followed by quantitative PCR (ChIP-qPCR). The numbers below indicate nucleotide positions relative to the ATG start codon. Black boxes represent exons; lines indicate introns, and white boxes denote the untranslated regions. **J** to **L**, ChIP-qPCR assay of the relative enrichment levels of H3Ac (**J**), H3K4Me3 (**K**), H3K27Me3 (**L**) at the *FLC* locus in wild type and *hos1-3*, *nup96-1*, *nup107-3*, *nup160-3*, and *nup85-1* mutants. Seedlings were grown in long days for 10 days. Values are means ± SD (n = 3 biological repeats). The *eIF4A* gene was used for normalizing the quantified DNA fragments. Statistical analysis was performed using Student's *t* test (*, $P < 0.05$).

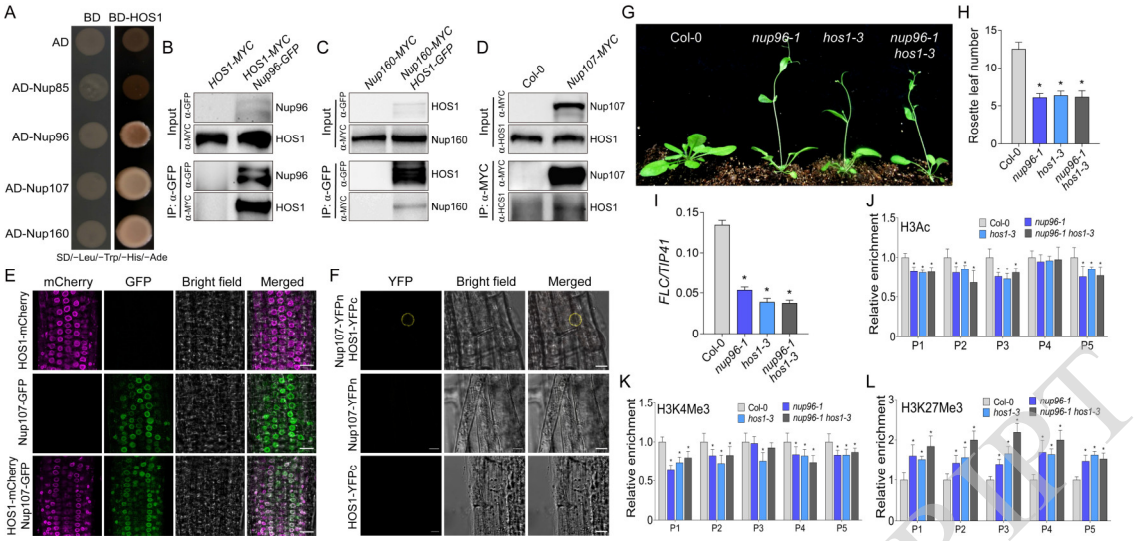

Fig. 3. Different Y-complex components interact with HOS1 to change histone modifications of *FLC* chromatin.

A, Yeast two-hybrid (Y2H) assay to detect interactions between HOS1 and Nup107–Nup160 sub-complex components. **B** to **D**, in vivo interaction of HOS1 with Nup96 (**B**), Nup160 (**C**), and Nup107 (**D**) in Arabidopsis. Plant total proteins extracted from 10-day transgenic seedlings grown in long days were immunoprecipitated with an anti-GFP antibody (**B** and **C**) or anti-MYC antibody (**D**) as indicated in each blot. The co-immunoprecipitated proteins were detected with anti-GFP, anti-MYC, or anti-HOS1 antibodies as indicated. **E**, Colocalization of Nup107-GFP and HOS1-mCherry in the roots of transgenic seedlings. Scale bars, 20 μm. **F**, Bimolecular fluorescence complementation (BiFC) assay showing HOS1 interacting with Nup107 in transgenic plants. HOS1 was fused to the C-terminal half of YFP (HOS1-YFPc), while Nup107 was fused to the N-terminal half of YFP (Nup107-YFPn). Scale bars, 10 μm. **G**, Flowering phenotypes of wild type, *nup96-1* and *hos1-3* single mutants, and the *nup96-1 hos1-3* double mutant grown in long-day conditions. **H**, Rosette leaf number at the time of flowering for the different genotypes shown in (**G**). Values are means ± SD (n ≥18). Statistical analysis was performed using Student's *t* test (*, $P < 0.05$). **I**, Relative *FLC* expression in wild-type, *nup96-1*, *hos1-3*, and *nup96-1 hos1-3* seedlings grown in long-day conditions. Values are means ± SD (n = 3 biological repeats). *TIP41* (At4g34270) was used as a reference gene. Statistical analysis was performed using Student's *t* test (*, $P < 0.05$). **J** to **L**, ChIP-qPCR analysis of relative enrichment levels of H3Ac (**J**), H3K4Me3 (**K**), H3K27Me3 (**L**) at the *FLC* locus in seedlings of wild type, *nup96-1* and the *hos1-3* single mutants and the *nup96-1 hos1-3* double mutant grown in long-day conditions for 10 days. Values are means ± SD (n = 3 biological repeats). The *eIF4A* gene was used for normalizing the quantified DNA fragments. Statistical analysis was performed using Student's *t* test (*, $P < 0.05$).

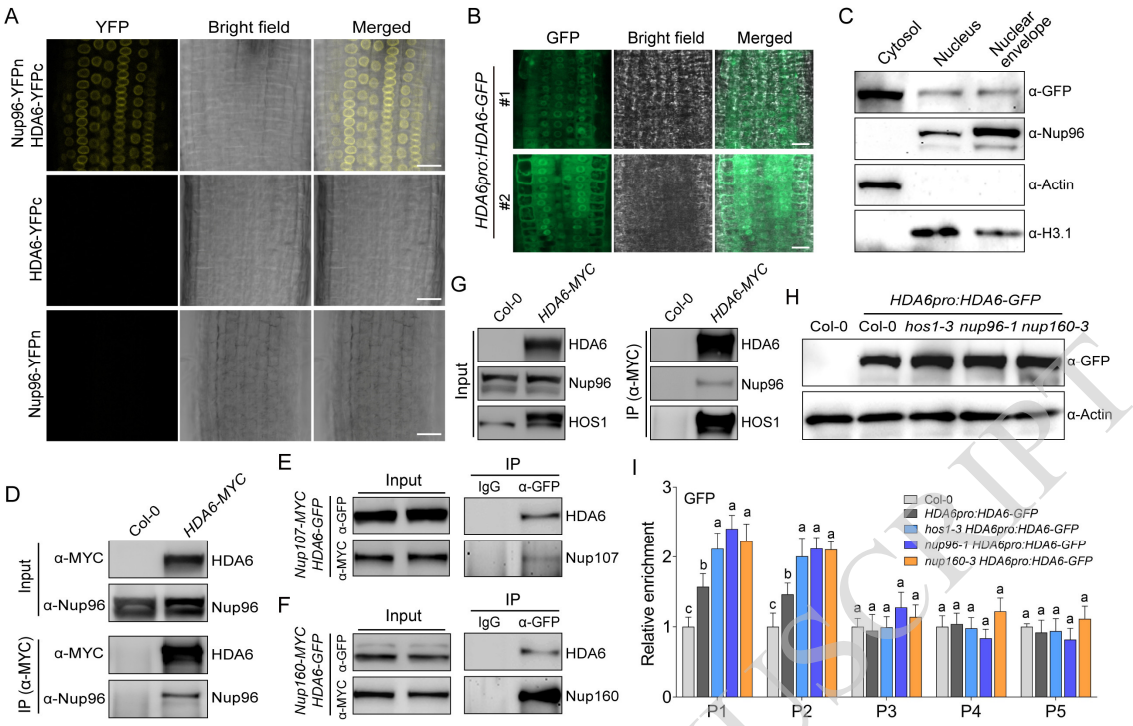

Fig. 4. Y-complex components associate with HDA6 to epigenetically modify histones over the *FLC* chromatin.

A, BiFC assay of HDA6-YFPc and Nup96-YFPn in the roots of transgenic seedlings. Scale bars, 20 μm. **B**, Subcellular distribution of HDA6-GFP in root epidermal cells of two *HDA6pro:HDA6-GFP* transgenic Arabidopsis seedlings (#1 and #2), showing high fluorescent signals at the nuclear rim. Scale bars, 20 μm. **C**, Immunoblotting on the purified nuclear envelope extracts of *HDA6pro:HDA6-GFP* transgenic lines compared to corresponding cytoplasm and nuclear samples and probed with the indicated antibodies. Nup96 was a positive control for the nuclear envelope fraction; histone H3.1 was a positive control for the nuclear fraction, and Actin was a positive control for the cytoplasmic fraction. **D**, In vivo interaction of Nup96 and HDA6 in *35S:HDA6-MYC* transgenic Arabidopsis lines. Cell extracts from 10-day-old seedlings were immunoprecipitated with an anti-MYC antibody. The precipitates were probed by immunoblotting with an anti-Nup96 antibody. **E** and **F** In vivo interaction of HDA6 with Nup107 (**E**), or Nup160 (**F**). Total proteins of *N. benthamiana* leaves co-expressing *HDA6-GFP* and *Nup107-MYC* (**E**) or *Nup160-MYC* (**F**) were immunoprecipitated with an anti-GFP antibody. The precipitates were probed by immunoblotting with an anti-MYC antibody. **G**, In vivo interaction assay of HDA6 with HOS1 and Nup96 in *35S:HDA6-MYC* transgenic lines. Cell extracts from 10-day-old seedlings were immunoprecipitated with an anti-MYC antibody. The precipitates were probed by immunoblotting with anti-Nup96 or anti-HOS1 antibodies. **H**, Immunoblotting analysis of HDA6-GFP in *HDA6pro:HDA6-GFP*, *hos1-3 HDA6pro:HDA6-GFP*, *nup96-1 HDA6pro:HDA6-GFP*, and *nup160-3 HDA6pro:HDA6-GFP* transgenic lines. **I**, ChIP-qPCR assay of relative enrichment levels of HDA6-GFP at the *FLC* locus in *HDA6pro:HDA6-GFP*, *hos1-3 HDA6pro:HDA6-GFP*, *nup96-1 HDA6pro:HDA6-GFP*, and *nup160-3 HDA6pro:HDA6-GFP* transgenic plants, using an anti-GFP antibody.

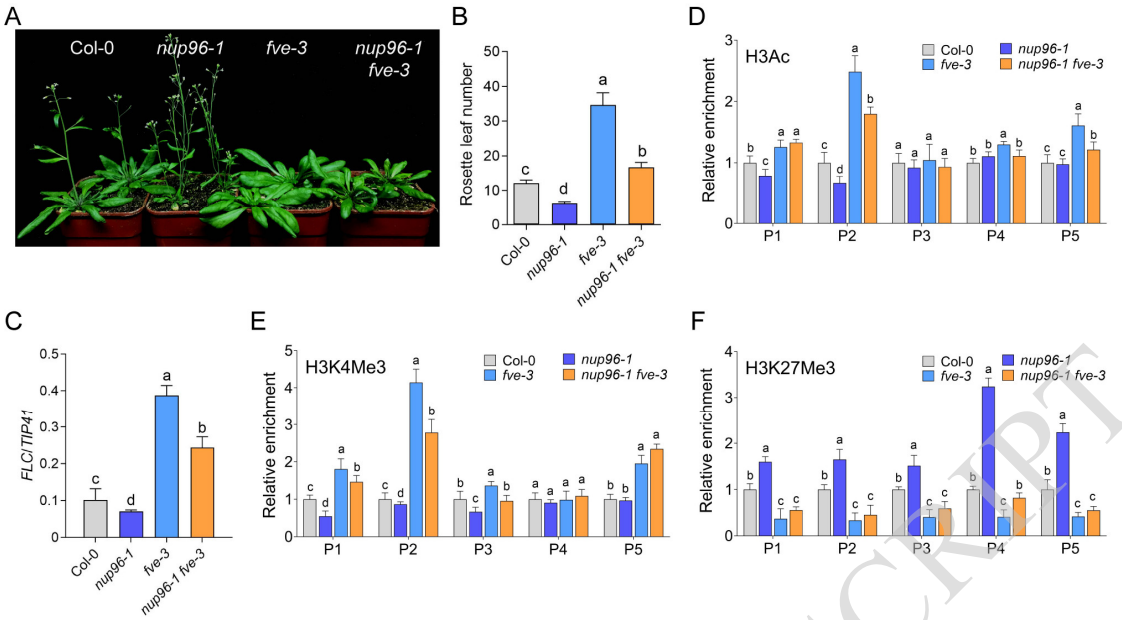

Fig. 5. Nup96 regulation of *FLC* chromatin modifications is associated with *FVE*.

A and **B**, Flowering phenotypes (**A**) and total rosette leaf number (**B**) of wild-type plants, *nup96-1* and *fve-3* single mutants, and the *nup96-1 fve-3* double mutant in long days. Values in (B) are means ± SD (n ≥ 18). **C**, Relative *FLC* expression in mutants and wild-type plants. Values are means ± SD (n = 3 biological repeats). **D** to **F**, ChIP-qPCR analysis of relative enrichment levels for H3Ac (**D**), H3K4Me3 (**E**), and H3K27Me3 (**F**) at the *FLC* locus in wild type, *nup96-1*, *fve-3*, and *nup96- fve-3*. Seedlings were grown in long-day conditions for 10 days. Values are means ± SD (n = 3 biological repeats). The *eIF4A* gene was used for normalizing the quantified DNA fragments while *TIP41* was used as a reference gene for RT-qPCR. Different lowercase letters indicate significant differences (*, $P < 0.05$) using one-way ANOVA.

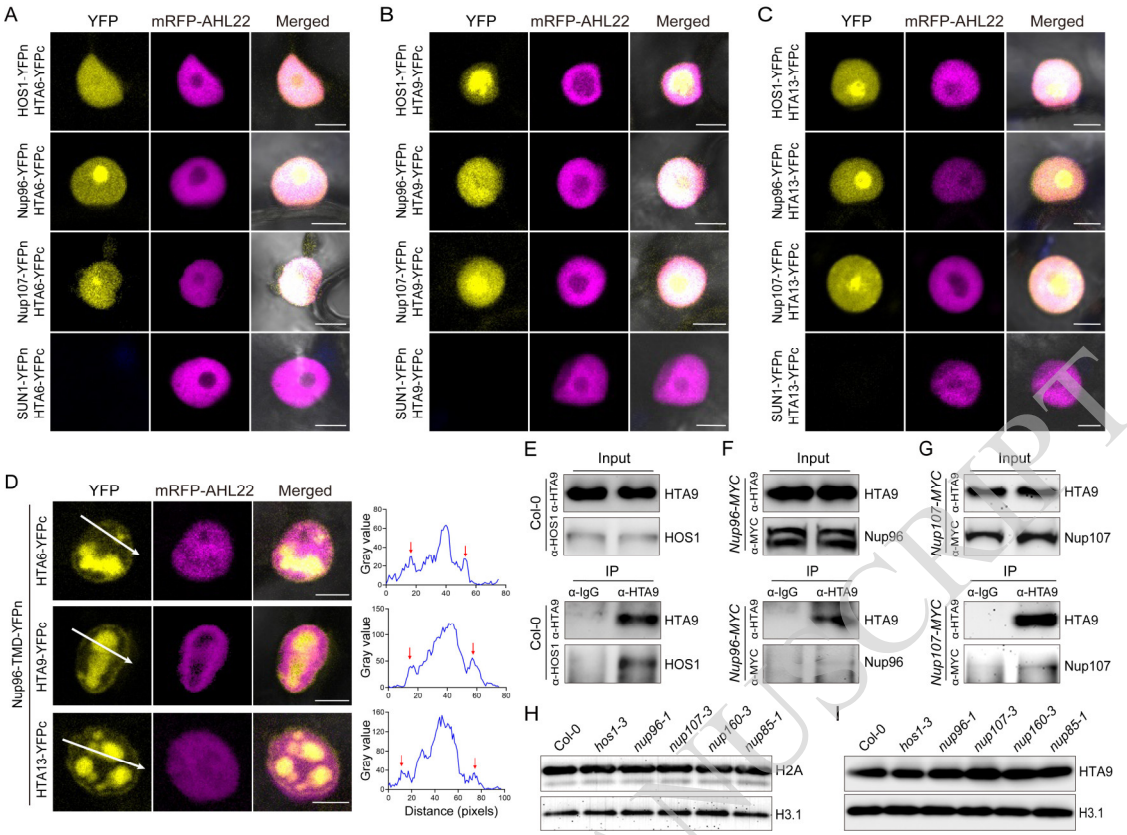

Fig. 6 The Y-complex is intimately associated with histone H2A proteins at the nuclear envelope.

A to **C**, BiFC assay of HTA6 **(A)**, HTA9 **(B)**, and HTA13 **(C)** interacting with different Y-complex components in *N. benthamiana.* HTAs were fused to the C-terminal half of YFP (HTA6-YFPc, HTA9-YFPc, HTA13-YFPc), while Y-complex components were fused to the N-terminal half of YFP (HOS1-YFPn, Nup96-YFPn, Nup107-YFPn). SUN1 (an inner nuclear membrane protein) served as negative control. mRFP-AHL22 served as a marker for nuclear localization. Scale bars, 10 μm. **D**, Left, BiFC assay of HTA6, HTA9, and HTA13 interacting with Nup96-TMD in *N. benthamiana*. mRFP-AHL22, served as a marker for nuclear localization. Right, measurement of YFP fluorescence intensity profiles along the lines indicated to the left. The peaks indicated by the red arrows represent the nuclear membrane positioning signal. Scale bars, 10 μm. **E** to **G**, In vivo interaction of HTA9 with HOS1 (**E**), Nup96 (**F**), and Nup107 (**G**) in Arabidopsis. Plant total proteins extracted from 10-day-old seedlings grown in long days were immunoprecipitated with an anti-HTA9 antibody. The co-immunoprecipitated proteins were probed with anti-HOS1 or anti-MYC antibody as indicated on the blots. **H** and **I**, Immunoblots showing the level of endogenous H2A (**H**) or HTA9 (**I**) in nuclear extracts from wild-type plants and different mutants. Histone H3.1 (H3.1) was used as the loading control.

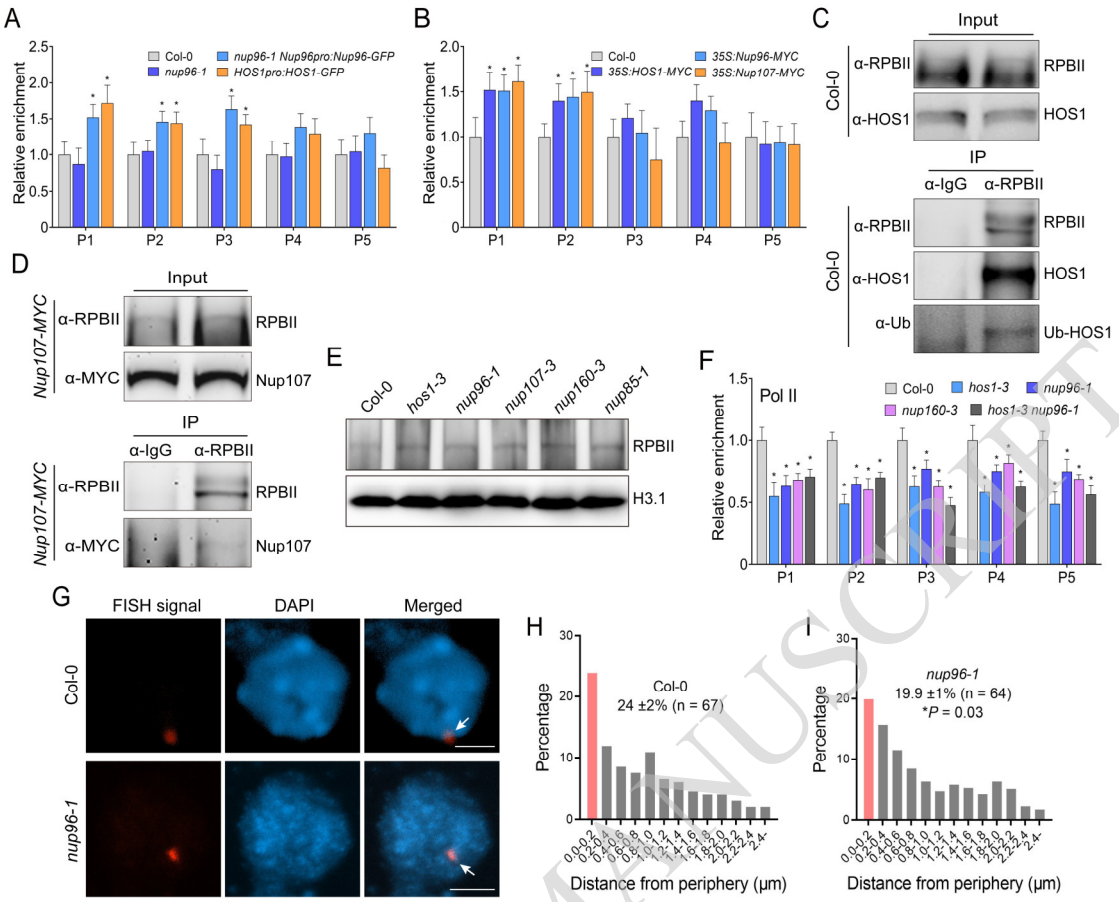

Fig. 7. The Nup107–Nup160 sub-complex regulates the position of the *FLC* locus in the nucleus.

A and **B**, ChIP-qPCR assay of the relative enrichment levels of Nup96, HOS1, and Nup107 proteins at the *FLC* locus in different transgenic plants with anti-GFP (**A**) or anti-MYC (**B**) antibodies. Seedlings were grown in long days for 10 days. **C** and **D**, In vivo interaction of RPBII with HOS1 (**C**) and Nup107 (**D**) in Arabidopsis. Plant total proteins extracted from 10-day seedlings grown in long days were immunoprecipitated by anti-RPBII antibodies. The co-immunoprecipitated proteins were probed with anti-HOS1, anti-MYC, or anti-Ubiquitin antibodies as indicated on the blots. **E**, Immunoblots showing the level of endogenous RPBII in nuclear extracts from wild-type plants and different mutants. Histone H3.1 (H3.1) was used as the loading control. **F**, ChIP-qPCR assay of the relative enrichment levels of RNA Pol II at the *FLC* locus in wild type, *hos1-3*, *nup96-1*, *nup160-3* and *hos1-3 nup96-1*. Seedlings were grown in long days for 10 days. **G**, Visualization of the *FLC* locus in the nucleus of wild type and *nup96-1* by fluorescence in situ hybridization (FISH). FISH signals are shown in red (white arrows); the nuclei were counterstained with DAPI (blue). Scale bars, 2 μm. **H** and **I**, Distribution of the *FLC* locus and average percentage of *FLC* locus localizing to the nuclear peripheral zone in wild type (**H**) and *nup96-1* (**I**). The red bars in the histogram represent the nuclear peripheral zone—the region from 0 μm to 0.2 μm from the nuclear edge. The average percentage of *FLC* loci within the nuclear peripheral zone with standard error (SE) from three independent replicates is shown. "n" represents the total number of FISH signals analyzed from all replicates. The *FLC* distribution data from the wild type was compared to that of *nup96-1* using a two-sided *t*-test, (*, $P < 0.05$).

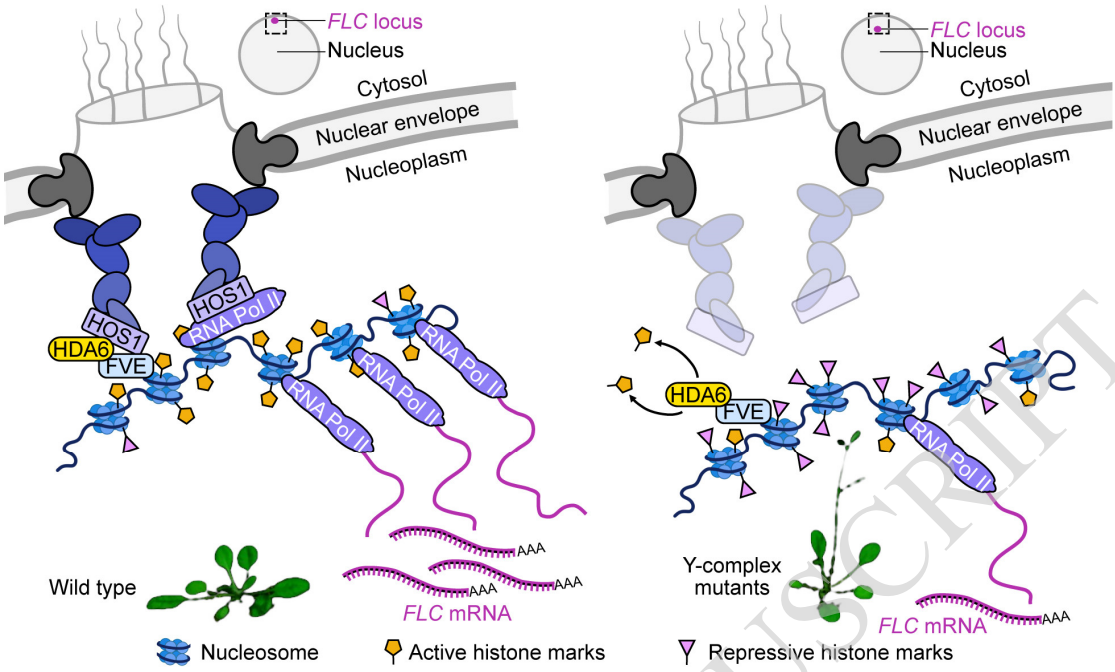

Fig. 8. A model for Y-complex function as a platform for *FLC* epigenetic modification conferring flowering regulation.

In wild-type plants, the intact Y-complex recruits *FLC* chromatin to the nuclear pore complex via interaction with histone proteins, and then facilitating RNA Pol II to be enriched on the chromatin and resulting in *FLC* expression. In Y-complex mutants, the recruitment of *FLC* chromatin is disrupted and the histone modification pattern is changed, leading to inhibition of *FLC* expression and early flowering.

Parsed Citations

Agote-Aran, A., Schmucker, S., Jerabkova, K., Jmel Boyer, I., Berto, A., Pacini, L., Ronchi, P., Kleiss, C., Guerard, L., Schwab, Y., Moine, H., Mandel, J.L., Jacquemont, S., Bagni, C., and Sumara, I. (2020). Spatial control of nucleoporin condensation by fragile X-related proteins. EMBO J 39, e104467.
Google Scholar: Author Only Title Only Author and Title

Allen, J.L., and Douglas, M.G. (1989). Organization of the nuclear pore complex in Saccharomyces cerevisiae. J Ultra struct Mol Struct Res 102, 95-108.
Google Scholar: Author Only Title Only Author and Title

Ausin, I., Alonso-Blanco, C., Jarillo, J.A., Ruiz-Garcia, L., and Martinez-Zapater, J.M. (2004). Regulation of flowering time by FVE, a retinoblastoma-associated protein. Nat Genet 36, 162-166.
Google Scholar: Author Only Title Only Author and Title

Bastow, R., Mylne, J.S., Lister, C., Lippman, Z., Martienssen, R.A., and Dean, C. (2004). Vernalization requires epigenetic silencing of FLC by histone methylation. Nature 427, 164-167.
Google Scholar: Author Only Title Only Author and Title

Berry, S., and Dean, C. (2015). Environmental perception and epigenetic memory: mechanistic insight through FLC. Plant J 83, 133-148.
Google Scholar: Author Only Title Only Author and Title

Bouche, F., Lobet, G., Tocquin, P., and Perilleux, C. (2016). FLOR-ID: an interactive database of flowering-time gene networks in Arabidopsis thaliana. Nucleic Acids Res 44, D1167-D1171.
Google Scholar: Author Only Title Only Author and Title

Cao, Y., Dai, Y., Cui, S., and Ma, L. (2008). Histone H2B monoubiquitination in the chromatin of FLOWERING LOCUS C regulates flowering time in Arabidopsis. Plant Cell 20, 2586-2602.
Google Scholar: Author Only Title Only Author and Title

Chakraborty, P., Wang, Y., Wei, J.H., van Deursen, J., Yu, H., Malureanu, L., Dasso, M., Forbes, D.J., Levy, D.E., Seemann, J., and Fontoura, B.M. (2008). Nucleoporin levels regulate cell cycle progression and phase-specific gene expression. Dev Cell 15, 657-667.
Google Scholar: Author Only Title Only Author and Title

Chen, Q.J., Zhou, H.M., Chen, J., and Wang, X.C. (2006). Using a modified TA cloning method to create entry clones. Anal Biochem 358, 120-125.
Google Scholar: Author Only Title Only Author and Title

Cheng, Z., Zhang, X., Huang, P., Huang, G., Zhu, J., Chen, F., Miao, Y., Liu, L., Fu, Y.F., and Wang, X. (2020). Nup96 and HOS1 Are Mutually Stabilized and Gate CONSTANS Protein Level, Conferring Long-Day Photoperiodic Flowering Regulation in Arabidopsis. Plant Cell 32, 374-391.
Google Scholar: Author Only Title Only Author and Title

Chow, K.H., Elgort, S., Dasso, M., Powers, M.A., and Ullman, K.S. (2014). The SUMO proteases SENP1 and SENP2 play a critical role in nucleoporin homeostasis and nuclear pore complex function. Mol Biol Cell 25, 160-168.
Google Scholar: Author Only Title Only Author and Title

Chytilova, E., Macas, J., Sliwinska, E., Rafelski, S.M., Lambert, G.M., and Galbraith, D.W. (2000). Nuclear dynamics in Arabidopsis thaliana. Mol Biol Cell 11, 2733-2741.
Google Scholar: Author Only Title Only Author and Title

D'Angelo, M.A. (2018). Nuclear pore complexes as hubs for gene regulation. Nucleus-Phila 9, 142-148.
Google Scholar: Author Only Title Only Author and Title

Deal, R.B., Topp, C.N., McKinney, E.C., and Meagher, R.B. (2007). Repression of flowering in Arabidopsis requires activation of FLOWERING LOCUS C expression by the histone variant H2A.Z. Plant Cell 19, 74-83.
Google Scholar: Author Only Title Only Author and Title

Dechat, T., Pfleghaar, K., Sengupta, K., Shimi, T., Shumaker, D.K., Solimando, L., and Goldman, R.D. (2008). Nuclear lamins: major factors in the structural organization and function of the nucleus and chromatin. Genes Dev 22, 832-853.
Google Scholar: Author Only Title Only Author and Title

DeGrasse, J.A., DuBois, K.N., Devos, D., Siegel, T.N., Sali, A., Field, M.C., Rout, M.P., and Chait, B.T. (2009). Evidence for a Shared Nuclear Pore Complex Architecture That Is Conserved from the Last Common Eukaryotic Ancestor. Mol Cell Proteomics 8, 2119-2130.
Google Scholar: Author Only Title Only Author and Title

Demmerle, J., Koch, A.J., and Holaska, J.M. (2013). Emerin and histone deacetylase 3 (HDAC3) cooperatively regulate expression

and nuclear positions of MyoD, Myf5, and Pax7 genes during myogenesis. Chromosome Res 21, 765-779.
Google Scholar: Author Only Title Only Author and Title

Dittmer, T.A., Stacey, N.J., Sugimoto-Shirasu, K., and Richards, E.J. (2007). LITTLE NUCLEI genes affecting nuclear morphology in Arabidopsis thaliana. Plant Cell 19, 2793-2803.
Google Scholar: Author Only Title Only Author and Title

Earley, K.W., Haag, J.R., Pontes, O., Opper, K., Juehne, T., Song, K.M., and Pikaard, C.S. (2006). Gateway-compatible vectors for plant functional genomics and proteomics. Plant J 45, 616-629.
Google Scholar: Author Only Title Only Author and Title

Feng, C.M., Qiu, Y.J., Van Buskirk, E.K., Yang, E.J., and Chen, M. (2014). Light-regulated gene repositioning in Arabidopsis. Nat Commun 5.
Google Scholar: Author Only Title Only Author and Title

Fiserova, J., Kiseleva, E., and Goldberg, M.W. (2009). Nuclear envelope and nuclear pore complex structure and organization in tobacco BY-2 cells. Plant J 59, 243-255.
Google Scholar: Author Only Title Only Author and Title

Gall, J.G. (1967). Octagonal nuclear pores. J Cell Biol 32, 391-399.
Google Scholar: Author Only Title Only Author and Title

Gao, N., Davuluri, G., Gong, W.L., Seiler, C., Lorent, K., Furth, E.E., Kaestner, K.H., and Pack, M. (2011). The Nuclear Pore Complex Protein Elys Is Required for Genome Stability in Mouse Intestinal Epithelial Progenitor Cells. Gastroenterology 140, 1547-U1252.
Google Scholar: Author Only Title Only Author and Title

Gao, X., Yu, S., Guan, Y., Shen, Y., and Xu, L. (2021). Nucleoporin 50 mediates Kcna4 transcription to regulate cardiac electrical activity. J Cell Sci 134.
Google Scholar: Author Only Title Only Author and Title

Geli, V., and Lisby, M. (2015). Recombinational DNA repair is regulated by compartmentalization of DNA lesions at the nuclear pore complex. Bioessays 37, 1287-1292.
Google Scholar: Author Only Title Only Author and Title

Goldberg, M.W., and Allen, T.D. (1996). The nuclear pore complex and lamina: three-dimensional structures and interactions determined by field emission in-lens scanning electron microscopy. J Mol Biol 257, 848-865.
Google Scholar: Author Only Title Only Author and Title

Goto, C., Hara-Nishimura, I., and Tamura, K. (2021). Regulation and Physiological Significance of the Nuclear Shape in Plants. Frontiers in plant science 12, 673905.
Google Scholar: Author Only Title Only Author and Title

Gozalo, A., Duke, A., Lan, Y., Pascual-Garcia, P., Talamas, J.A., Nguyen, S.C., Shah, P.P., Jain, R., Joyce, E.F., and Capelson, M. (2020). Core Components of the Nuclear Pore Bind Distinct States of Chromatin and Contribute to Polycomb Repression. Mol Cell 77, 67-81 e67.
Google Scholar: Author Only Title Only Author and Title

Griffis, E.R., Xu, S., and Powers, M.A. (2003). Nup98 localizes to both nuclear and cytoplasmic sides of the nuclear pore and binds to two distinct nucleoporin subcomplexes. Mol Biol Cell 14, 600-610.
Google Scholar: Author Only Title Only Author and Title

Groves, N.R., McKenna, J.F., Evans, D.E., Graumann, K., and Meier, I. (2019). A nuclear localization signal targets tail-anchored membrane proteins to the inner nuclear envelope in plants. J Cell Sci 132.
Google Scholar: Author Only Title Only Author and Title

Gu, X., Jiang, D., Yang, W., Jacob, Y., Michaels, S.D., and He, Y. (2011a). Arabidopsis homologs of retinoblastoma-associated protein 46/48 associate with a histone deacetylase to act redundantly in chromatin silencing. PLoS genetics 7, e1002366.
Google Scholar: Author Only Title Only Author and Title

Gu, X.F., Jiang, D.H., Yang, W.N., Jacob, Y., Michaels, S.D., and He, Y.H. (2011b). Arabidopsis Homologs of Retinoblastoma-Associated Protein 46/48 Associate with a Histone Deacetylase to Act Redundantly in Chromatin Silencing. Plos Genet 7.
Google Scholar: Author Only Title Only Author and Title

Gu, Y. (2018). The nuclear pore complex: a strategic platform for regulating cell signaling. New Phytol 219, 25-30.
Google Scholar: Author Only Title Only Author and Title

Gutierrez, L., Mauriat, M., Guenin, S., Pelloux, J., Lefebvre, J.F., Louvet, R., Rusterucci, C., Moritz, T., Guerineau, F., Bellini, C., and Van Wuytswinkel, O. (2008). The lack of a systematic validation of reference genes: a serious pitfall undervalued in reverse transcription-polymerase chain reaction (RT-PCR) analysis in plants. Plant Biotechnol J 6, 609-618.

Google Scholar: Author Only Title Only Author and Title

Hayama, R., Sarid-Krebs, L., Richter, R., Fernandez, V., Jang, S., and Coupland, G. (2017). PSEUDO RESPONSE REGULATORs stabilize CONSTANS protein to promote flowering in response to day length. Embo J 36, 904-918.
Google Scholar: Author Only Title Only Author and Title

He, Y., Michaels, S.D., and Amasino, R.M. (2003). Regulation of flowering time by histone acetylation in Arabidopsis. Science 302, 1751-1754.
Google Scholar: Author Only Title Only Author and Title

He, Y., Doyle, M.R., and Amasino, R.M. (2004). PAF1-complex-mediated histone methylation of FLOWERING LOCUS C chromatin is required for the vernalization-responsive, winter-annual habit in Arabidopsis. Genes Dev 18, 2774-2784.
Google Scholar: Author Only Title Only Author and Title

Hepworth, J., and Dean, C. (2015). Flowering Locus C's Lessons: Conserved Chromatin Switches Underpinning Developmental Timing and Adaptation. Plant Physiol 168, 1237-1245.
Google Scholar: Author Only Title Only Author and Title

Huang, X., Zhang, Q., Jiang, Y.P., Yang, C.W., Wang, Q.Y., and Li, L. (2018). Shade-induced nuclear localization of PIF7 is regulated by phosphorylation and 14-3-3 proteins in Arabidopsis. Elife 7.
Google Scholar: Author Only Title Only Author and Title

Ibarra, A., and Hetzer, M.W. (2015). Nuclear pore proteins and the control of genome functions. Genes Dev 29, 337-349.
Google Scholar: Author Only Title Only Author and Title

Jacinto, F.V., Benner, C., and Hetzer, M.W. (2015). The nucleoporin Nup153 regulates embryonic stem cell pluripotency through gene silencing. Gene Dev 29, 1224-1238.
Google Scholar: Author Only Title Only Author and Title

Jacob, Y., Mongkolsiriwatana, C., Veley, K.M., Kim, S.Y., and Michaels, S.D. (2007). The nuclear pore protein AtTPR is required for RNA homeostasis, flowering time, and auxin signaling. Plant Physiol 144, 1383-1390.
Google Scholar: Author Only Title Only Author and Title

Jeon, J., and Kim, J. (2011). FVE, an Arabidopsis Homologue of the Retinoblastoma-Associated Protein That Regulates Flowering Time and Cold Response, Binds to Chromatin as a Large Multiprotein Complex. Mol Cells 32, 227-234.
Google Scholar: Author Only Title Only Author and Title

Jiang, S., Xiao, L., Huang, P., Cheng, Z., Chen, F., Miao, Y., Fu, Y.F., Chen, Q., and Zhang, X.M. (2019). Nucleoporin Nup98 participates in flowering regulation in a CONSTANS-independent mode. Plant Cell Rep 38, 1263-1271.
Google Scholar: Author Only Title Only Author and Title

Jung, H., Yan, J., Zhai, Z., and Vatamaniuk, O.K. (2015). Gene functional analysis using protoplast transient assays. Methods Mol Biol 1284, 433-452.
Google Scholar: Author Only Title Only Author and Title

Jung, J.H., Park, J.H., Lee, S., To, T.K., Kim, J.M., Seki, M., and Park, C.M. (2013). The cold signaling attenuator HIGH EXPRESSION OF OSMOTICALLY RESPONSIVE GENE1 activates FLOWERING LOCUS C transcription via chromatin remodeling under short-term cold stress in Arabidopsis. Plant Cell 25, 4378-4390.
Google Scholar: Author Only Title Only Author and Title

Kim, J.M., To, T.K., and Seki, M. (2012). An epigenetic integrator: new insights into genome regulation, environmental stress responses and developmental controls by histone deacetylase 6. Plant Cell Physiol 53, 794-800.
Google Scholar: Author Only Title Only Author and Title

Koornneef, M., Hanhart, C.J., and van der Veen, J.H. (1991). A genetic and physiological analysis of late flowering mutants in Arabidopsis thaliana. Mol Gen Genet 229, 57-66.
Google Scholar: Author Only Title Only Author and Title

Koornneef, M., Alonso-Blanco, C., Blankestijn-de Vries, H., Hanhart, C.J., and Peeters, A.J.M. (1998). Genetic interactions among late-flowering mutants of Arabidopsis. Genetics 148, 885-892.
Google Scholar: Author Only Title Only Author and Title

Kosak, S.T., Skok, J.A., Medina, K.L., Riblet, R., Le Beau, M.M., Fisher, A.G., and Singh, H. (2002). Subnuclear compartmentalization of immunoglobulin loci during lymphocyte development. Science 296, 158-162.
Google Scholar: Author Only Title Only Author and Title

Kuhn, T.M., and Capelson, M. (2019). Nuclear Pore Proteins in Regulation of Chromatin State. Cells-Basel 8.
Google Scholar: Author Only Title Only Author and Title

Lee, H., Xiong, L., Gong, Z., Ishitani, M., Stevenson, B., and Zhu, J.K. (2001). The Arabidopsis HOS1 gene negatively regulates cold signal transduction and encodes a RING finger protein that displays cold-regulated nucleo--cytoplasmic partitioning. Genes

Dev 15, 912-924.
Google Scholar: Author Only Title Only Author and Title

Lee, J.H., Yoo, S.J., Park, S.H., Hwang, I., Lee, J.S., and Ahn, J.H. (2007). Role of SVP in the control of flowering time by ambient temperature in Arabidopsis. Genes Dev 21, 397-402.
Google Scholar: Author Only Title Only Author and Title

Lee, J.H., Kim, J.J., Kim, S.H., Cho, H.J., Kim, J., and Ahn, J.H. (2012). The E3 ubiquitin ligase HOS1 regulates low ambient temperature-responsive flowering in Arabidopsis thaliana. Plant Cell Physiol 53, 1802-1814.
Google Scholar: Author Only Title Only Author and Title

Lei, B.K., and Berger, F. (2020). H2A Variants in Arabidopsis: Versatile Regulators of Genome Activity. Plant Communications 1.
Google Scholar: Author Only Title Only Author and Title

Li, C., Liu, L., Teo, Z.W.N., Shen, L., and Yu, H. (2020). Nucleoporin 160 Regulates Flowering through Anchoring HOS1 for Destabilizing CO in Arabidopsis. Plant Commun 1, 100033.
Google Scholar: Author Only Title Only Author and Title

Li, D., Liu, C., Shen, L., Wu, Y., Chen, H., Robertson, M., Helliwell, C.A., Ito, T., Meyerowitz, E., and Yu, H. (2008). A repressor complex governs the integration of flowering signals in Arabidopsis. Dev Cell 15, 110-120.
Google Scholar: Author Only Title Only Author and Title

Li, X., and Gu, Y.N. (2020). Structural and functional insight into the nuclear pore complex and nuclear transport receptors in plant stress signaling. Current Opinion in Plant Biology 58, 60-68.
Google Scholar: Author Only Title Only Author and Title

Lin, D.H., and Hoelz, A. (2019). The Structure of the Nuclear Pore Complex (An Update). Annu Rev Biochem 88, 725-783.
Google Scholar: Author Only Title Only Author and Title

Liu, F., Quesada, V., Crevillen, P., Baurle, I., Swiezewski, S., and Dean, C. (2007). The Arabidopsis RNA-binding protein FCA requires a lysine-specific demethylase 1 homolog to downregulate FLC. Mol Cell 28, 398-407.
Google Scholar: Author Only Title Only Author and Title

Liu, X., Luo, M., and Wu, K. (2012a). Epigenetic interplay of histone modifications and DNA methylation mediated by HDA6. Plant signaling & behavior 7, 633-635.
Google Scholar: Author Only Title Only Author and Title

Liu, X.C., Yu, C.W., Duan, J., Luo, M., Wang, K.C., Tian, G., Cui, Y.H., and Wu, K.Q. (2012b). HDA6 Directly Interacts with DNA Methyltransferase MET1 and Maintains Transposable Element Silencing in Arabidopsis. Plant Physiology 158, 119-129.
Google Scholar: Author Only Title Only Author and Title

Liu, Z.X., Yan, M.B., Liang, Y.J., Liu, M., Zhang, K., Shao, D.D., Jiang, R.C., Li, L., Wang, C.M., Nussenzveig, D.R., Zhang, K.K., Chen, S.X., Zhong, C.Q., Mo, W., Fontoura, B.M.A., and Zhang, L. (2019). Nucleoporin Seh1 Interacts with Olig2/Brd7 to Promote Oligodendrocyte Differentiation and Myelination. Neuron 102, 587-+.
Google Scholar: Author Only Title Only Author and Title

Loiodice, I., Alves, A., Rabut, G., Van Overbeek, M., Ellenberg, J., Sibarita, J.B., and Doye, V. (2004). The entire Nup107-160 complex, including three new members, is targeted as one entity to kinetochores in mitosis. Mol Biol Cell 15, 3333-3344.
Google Scholar: Author Only Title Only Author and Title

Meier, I., Richards, E.J., and Evans, D.E. (2017). Cell Biology of the Plant Nucleus. Annu Rev Plant Biol 68, 139-172.
Google Scholar: Author Only Title Only Author and Title

Meister, P., Towbin, B.D., Pike, B.L., Ponti, A., and Gasser, S.M. (2010). The spatial dynamics of tissue-specific promoters during C-elegans development. Gene Dev 24, 766-782.
Google Scholar: Author Only Title Only Author and Title

Michaels, S.D., and Amasino, R.M. (1999). FLOWERING LOCUS C encodes a novel MADS domain protein that acts as a repressor of flowering. Plant Cell 11, 949-956.
Google Scholar: Author Only Title Only Author and Title

Morchoisne-Bolhy, S., Geoffroy, M.C., Bouhlel, I.B., Alves, A., Auduge, N., Baudin, X., Van Bortle, K., Powers, M.A., and Doye, V. (2015). Intranuclear dynamics of the Nup107-160 complex. Mol Biol Cell 26, 2343-2356.
Google Scholar: Author Only Title Only Author and Title

Niu, Y.X., Bai, J.T., Liu, X.Y., Zhang, H., Bao, J.P., Zhao, W.S., Hou, Y.F., Deng, X., Yang, C., Guo, L., Geng, Z.Y., Xie, H.L., Wu, H.Y., Shen, M., Lou, X.J., Tang, W.Q., Liu, X.G., Sun, D.Y., Cao, X.F., and Zheng, S.Z. (2022). HISTONE DEACETYLASE 9 transduces heat signal in plant cells. P Natl Acad Sci USA 119.
Google Scholar: Author Only Title Only Author and Title

Parry, G. (2014). Components of the Arabidopsis nuclear pore complex play multiple diverse roles in control of plant growth. J

Exp Bot 65, 6057-6067.
Google Scholar: Author Only Title Only Author and Title

Parry, G., Ward, S., Cernac, A., Dharmasiri, S., and Estelle, M. (2006). The Arabidopsis SUPPRESSOR OF AUXIN RESISTANCE proteins are nucleoporins with an important role in hormone signaling and development. Plant Cell 18, 1590-1603.
Google Scholar: Author Only Title Only Author and Title

Ptak, C., and Wozniak, R.W. (2016). Nucleoporins and chromatin metabolism. Curr Opin Cell Biol 40, 153-160.
Google Scholar: Author Only Title Only Author and Title

Ragoczy, T., Bender, M.A., Telling, A., Byron, R., and Groudine, M. (2006). The locus control region is required for association of the murine beta-globin locus with engaged transcription factories during erythroid maturation. Gene Dev 20, 1447-1457.
Google Scholar: Author Only Title Only Author and Title

Rajoo, S., Vallotton, P., Onischenko, E., and Weis, K. (2018). Stoichiometry and compositional plasticity of the yeast nuclear pore complex revealed by quantitative fluorescence microscopy. Proc Natl Acad Sci U S A 115, E3969-E3977.
Google Scholar: Author Only Title Only Author and Title

Rosa, S., Duncan, S., and Dean, C. (2016). Mutually exclusive sense-antisense transcription at FLC facilitates environmentally induced gene repression. Nat Commun 7, 13031.
Google Scholar: Author Only Title Only Author and Title

Rosa, S., De Lucia, F., Mylne, J.S., Zhu, D., Ohmido, N., Pendle, A., Kato, N., Shaw, P., and Dean, C. (2013). Physical clustering of FLC alleles during Polycomb-mediated epigenetic silencing in vernalization. Gene Dev 27, 1845-1850.
Google Scholar: Author Only Title Only Author and Title

Sakamoto, Y., Sato, M., Sato, Y., Harada, A., Suzuki, T., Goto, C., Tamura, K., Toyooka, K., Kimura, H., Ohkawa, Y., Hara-Nishimura, I., Takagi, S., and Matsunaga, S. (2020). Subnuclear gene positioning through lamina association affects copper tolerance. Nature communications 11, 5914.
Google Scholar: Author Only Title Only Author and Title

Salas-Pino, S., Gallardo, P., Barrales, R.R., Braun, S., and Daga, R.R. (2017). The fission yeast nucleoporin Alm1 is required for proteasomal degradation of kinetochore components. Journal of Cell Biology 216, 3591-3608.
Google Scholar: Author Only Title Only Author and Title

Saleh, A., Alvarez-Venegas, R., and Avramova, Z. (2008). An efficient chromatin immunoprecipitation (ChIP) protocol for studying histone modifications in Arabidopsis plants. Nat Protoc 3, 1018-1025.
Google Scholar: Author Only Title Only Author and Title

Seo, E., Lee, H., Jeon, J., Park, H., Kim, J., Noh, Y.S., and Lee, I. (2009). Crosstalk between Cold Response and Flowering in Arabidopsis Is Mediated through the Flowering-Time Gene SOC1 and Its Upstream Negative Regulator FLC. Plant Cell 21, 3185-3197.
Google Scholar: Author Only Title Only Author and Title

Simpson, G.G. (2004). The autonomous pathway: epigenetic and post-transcriptional gene regulation in the control of Arabidopsis flowering time. Curr Opin Plant Biol 7, 570-574.
Google Scholar: Author Only Title Only Author and Title

Smith, S., Galinha, C., Desset, S., Tolmie, F., Evans, D., Tatout, C., and Graumann, K. (2015). Marker gene tethering by nucleoporins affects gene expression in plants. Nucleus 6, 471-478.
Google Scholar: Author Only Title Only Author and Title

Sura, W., Kabza, M., Karlowski, W.M., Bieluszewski, T., Kus-Slowinska, M., Paweloszek, L., Sadowski, J., and Ziolkowski, P.A. (2017). Dual Role of the Histone Variant H2A.Z in Transcriptional Regulation of Stress-Response Genes. Plant Cell 29, 791-807.
Google Scholar: Author Only Title Only Author and Title

Talbert, P.B., and Henikoff, S. (2010). Histone variants - ancient wrap artists of the epigenome. Nat Rev Mol Cell Bio 11, 264-275.
Google Scholar: Author Only Title Only Author and Title

Tamura, K. (2020). Nuclear pore complex-mediated gene expression in Arabidopsis thaliana. J Plant Res 133, 449-455.
Google Scholar: Author Only Title Only Author and Title

Tamura, K., and Hara-Nishimura, I. (2011). Involvement of the nuclear pore complex in morphology of the plant nucleus. Nucleus-Phila 2, 168-172.
Google Scholar: Author Only Title Only Author and Title

Tamura, K., Fukao, Y., Iwamoto, M., Haraguchi, T., and Hara-Nishimura, I. (2010). Identification and characterization of nuclear pore complex components in Arabidopsis thaliana. Plant Cell 22, 4084-4097.
Google Scholar: Author Only Title Only Author and Title

Tang, Y., Dong, Q., Wang, T., Gong, L., and Gu, Y. (2021). PNET2 is a component of the plant nuclear lamina and is required for

proper genome organization and activity. Dev Cell.
Google Scholar: Author Only Title Only Author and Title

Vaquerizas, J.M., Suyama, R., Kind, J., Miura, K., Luscombe, N.M., and Akhtar, A. (2010). Nuclear pore proteins nup153 and megator define transcriptionally active regions in the Drosophila genome. PLoS genetics 6, e1000846.
Google Scholar: Author Only Title Only Author and Title

Walther, T.C., Alves, A., Pickersgill, H., Loiodice, I., Hetzer, M., Galy, V., Hulsmann, B.B., Kocher, T., Wilm, M., Allen, T., Mattaj, I.W., and Doye, V. (2003). The conserved Nup107-160 complex is critical for nuclear pore complex assembly. Cell 113, 195-206.
Google Scholar: Author Only Title Only Author and Title

Wang, X., Fan, C.M., Zhang, X.M., Zhu, J.L., and Fu, Y.F. (2013). BioVector, a flexible system for gene specific-expression in plants. Bmc Plant Biol 13.
Google Scholar: Author Only Title Only Author and Title

Whittaker, C., and Dean, C. (2017). The FLC Locus: A Platform for Discoveries in Epigenetics and Adaptation. Annu Rev Cell Dev Biol 33, 555-575.
Google Scholar: Author Only Title Only Author and Title

Wong, R.W., Mamede, J.I., and Hope, T.J. (2015). Impact of Nucleoporin-Mediated Chromatin Localization and Nuclear Architecture on HIV Integration Site Selection. J Virol 89, 9702-9705.
Google Scholar: Author Only Title Only Author and Title

Wong, X., Melendez-Perez, A.J., and Reddy, K.L. (2022). The Nuclear Lamina. Cold Spring Harbor perspectives in biology 14, a040113.
Google Scholar: Author Only Title Only Author and Title

Wu, K., Zhang, L., Zhou, C., Yu, C.W., and Chaikam, V. (2008). HDA6 is required for jasmonate response, senescence and flowering in Arabidopsis. J Exp Bot 59, 225-234.
Google Scholar: Author Only Title Only Author and Title

Wu, X.S., Kasper, L.H., Mantcheva, R.T., Mantchev, G.T., Springett, M.J., and van Deursen, J.M.A. (2001). Disruption of the FG nucleoporin NUP98 causes selective changes in nuclear pore complex stoichiometry and function. P Natl Acad Sci USA 98, 3191-3196.
Google Scholar: Author Only Title Only Author and Title

Wu, Z., Fang, X.F., Zhu, D.L., and Deati, C. (2020). Autonomous Pathway: FLOWERING LOCUS C Repression through an Antisense-Mediated Chromatin-Silencing Mechanism. Plant Physiology 182, 27-37.
Google Scholar: Author Only Title Only Author and Title

Xiao, L., Liu, W., Chen, F., Zhang, X., Chen, Q., and Fu, Y.-F. (2016). The Phenotype Analysis of NUP107-160 Subcomplex Mutants in Arabidopsis. J. Agri. Sci. Tech. 18, 54-61.
Google Scholar: Author Only Title Only Author and Title

Xiao, L., Jiang, S., Huang, P., Chen, F., Wang, X., Cheng, Z., Miao, Y., Liu, L., Searle, I., Liu, C., Wu, X.X., Fu, Y.F., Chen, Q., and Zhang, X.M. (2020). Two Nucleoporin98 homologous genes jointly participate in the regulation of starch degradation to repress senescence in Arabidopsis. Bmc Plant Biol 20, 292.
Google Scholar: Author Only Title Only Author and Title

Xu, X.M., Rose, A., Muthuswamy, S., Jeong, S.Y., Venkatakrishnan, S., Zhao, Q., and Meier, I. (2007). NUCLEAR PORE ANCHOR, the Arabidopsis homolog of Tpr/Mlp1/Mlp2/megator, is involved in mRNA export and SUMO homeostasis and affects diverse aspects of plant development. Plant Cell 19, 1537-1548.
Google Scholar: Author Only Title Only Author and Title

Yang, H.C., Howard, M., and Dean, C. (2014). Antagonistic Roles for H3K36me3 and H3K27me3 in the Cold-Induced Epigenetic Switch at Arabidopsis FLC. Current Biology 24, 1793-1797.
Google Scholar: Author Only Title Only Author and Title

Yu, C.W., Chang, K.Y., and Wu, K.Q. (2016). Genome-Wide Analysis of Gene Regulatory Networks of the FVE-HDA6-FLD Complex in Arabidopsis. Frontiers in plant science 7.
Google Scholar: Author Only Title Only Author and Title

Yu, C.W., Liu, X., Luo, M., Chen, C., Lin, X., Tian, G., Lu, Q., Cui, Y., and Wu, K. (2011). HISTONE DEACETYLASE6 interacts with FLOWERING LOCUS D and regulates flowering in Arabidopsis. Plant Physiol 156, 173-184.
Google Scholar: Author Only Title Only Author and Title

Yu, X., and Michaels, S.D. (2010). The Arabidopsis Paf1c complex component CDC73 participates in the modification of FLOWERING LOCUS C chromatin. Plant Physiol 153, 1074-1084.
Google Scholar: Author Only Title Only Author and Title

Zhang, Y., and Li, X. (2005). A putative nucleoporin 96 Is required for both basal defense and constitutive resistance responses mediated by suppressor of npr1-1,constitutive 1. Plant Cell 17, 1306-1316.
Google Scholar: Author Only Title Only Author and Title

Zhao, Z., Yu, Y., Meyer, D., Wu, C., and Shen, W.H. (2005). Prevention of early flowering by expression of FLOWERING LOCUS C requires methylation of histone H3 K36. Nature cell biology 7, 1256-1260.
Google Scholar: Author Only Title Only Author and Title

Zhou, X., Graumann, K., Evans, D.E., and Meier, I. (2012). Novel plant SUN-KASH bridges are involved in RanGAP anchoring and nuclear shape determination. J Cell Biol 196, 203-211.
Google Scholar: Author Only Title Only Author and Title

Zhu, Y., Wang, B., Tang, K., Hsu, C.C., Xie, S., Du, H., Yang, Y., Tao, W.A., and Zhu, J.K. (2017). An Arabidopsis Nucleoporin NUP85 modulates plant responses to ABA and salt stress. PLoS genetics 13, e1007124.
Google Scholar: Author Only Title Only Author and Title

Zilberman, D., Coleman-Derr, D., Ballinger, T., and Henikoff, S. (2008). Histone H2A.Z and DNA methylation are mutually antagonistic chromatin marks. Nature 456, 125-U114.
Google Scholar: Author Only Title Only Author and Title